Chapter 2

Application of CNTs Gas Sensor in Online Monitoring of SF_6 Insulated Equipment

Xiaoxing Zhang, Song Xiao, Ju Tang and Cheng Pan

Additional information is available at the end of the chapter

http://dx.doi.org/10.5772/intechopen.68325

Abstract

The detection and analysis of SF_6 decomposition components are of great significance in online condition assessment and fault diagnosis of GIS. Considering the shortcomings of general detection methods, carbon nanotubes (CNTs) gas sensor was studied to detect the SF_6 decomposition components because of its advantages in large surface activity and abundant pore structure, et al. The large surface area has a strong adsorption and desorption capacity. In this chapter, SF_6 decomposed gases, namely SO_2F_2, SOF_2, SO_2, H_2S and CF_4 are chosen as probe gases because they are the main by-products in the decomposition of SF_6 under partial density (PD). First, the properties and preparation methods of CNTs are introduced to verify the advantages of CNTs for SF_6 decomposition components detection. Then, both theoretical calculation and sensing experiment were adopted to study the microadsorption mechanism and macrogas-sensing properties. Based on the intrinsic CNTs, study for SF_6 decomposition components adsorption, Pd, Ni, Al, Pt and Au metal doping CNTs and plasma-modified CNTs are discussed in order to enhance the gas sensing and selectivity of CNTs.

Keywords: SF_6 decomposition components, carbon nanotubes, preparation method, density functional theory, metal doping

1. Introduction of carbon nanotubes

1.1. The properties of carbon nanotubes

1.1.1. Structure of carbon nanotubes

Carbon nanotubes (CNTs), which are also called the bucky tube, are a one-dimensional material with special structure. It is one allotrope of carbon, like the diamond, graphite and

fullerene. In January 1991, a Japanese physicist Iijima first found CNTs produced during fabricating Carbon fiber using high-resolution transmission electron microscope [1]. CNTs possess large aspect ratio because of its one-dimensional property. The electron wave function of CNTs exhibits periodic and translational invariance in radial and axial direction. A new strong atomic hybrid orbital is built by sp^2 hybridization of carbon atoms, and CNTs skeleton of a hexagonal honeycomb is combined by σ bonds of carbon atoms. The isolated p electrons of Carbon atoms that did not participate in a hybrid together form conjugated π electron cloud across the entire CNTs. As shown in **Figure 1**, CNTs can be divided into single-wall carbon nanotubes (SWCNTs) and multi-wall carbon nanotubes (MWCNTs). Due to the unique molecular structure, CNTs have some specific properties in mechanics, electricity and heat.

1.1.2. Mechanical properties of carbon nanotubes

Carbon atoms in CNTs show sp^2 hybridization, which have more s orbital compared with sp^3 hybridization, and hence, the formed CNTs possess high modulus and strength. Its hardness is similar to that of diamond, while it also can be stretched due to its good flexibility. Like the reinforced fiber used in industry, the crucial factor that determines the strength of fiber is length to diameter ratio (at least 20:1). And the length to diameter ratio of CNTs has even

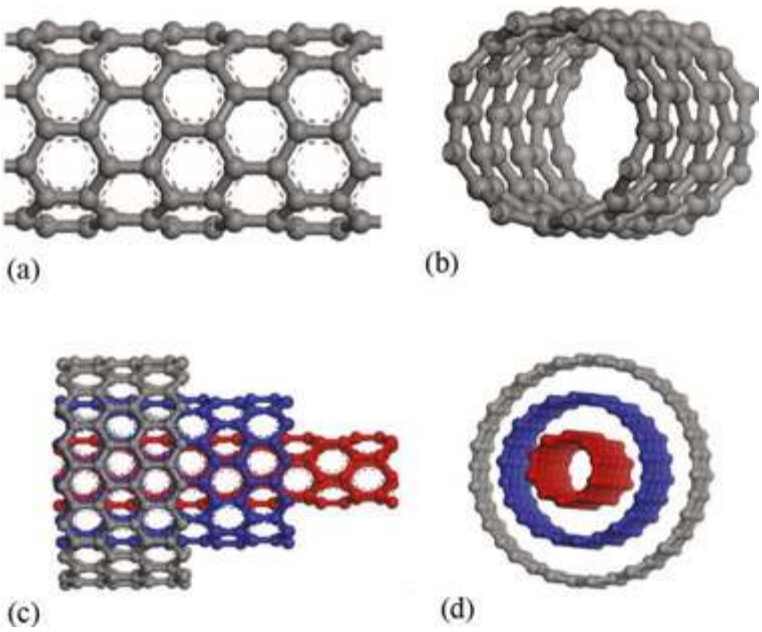

Figure 1. CNTs structural models. (a) SWCNTs (lateral view); (b) SWCNTs (sectional view); (c) MWCNTs (lateral view); (d) MWCNTs (sectional view).

reached 1000:1, making it an ideal fiber material with high strength, while the weight of CNTs is only 1/6–1/7 that of steel [2]. Therefore, CNTs are also called "super fiber". Besides, Krishnan et al. found that the Young's modulus of SWCNTs along radial direction is up to 1 TPa measured by atomic force microscope [3].

1.1.3. The thermal properties of carbon nanotubes

CNTs show heat conduction anisotropy, showing high and low heat exchange in vertical and axial direction, respectively. Therefore, the high anisotropy of heat conduction material can be synthesized by controlling the orientation of the CNTs. The thermal conductivity of composites can be effectively improved by doping trace of CNTs.

1.1.4. The electrical properties of CNTs

The isolated p electrons of C atoms do not participate in a hybridization form a wide range of delocalized π bond due to the significant conjugative effect, making it possesses special electrical properties. As shown in **Figure 2**, C_h represents the arrangement direction of CNTs atom, while a_1 and a_2 represent two basis vectors, respectively, where $C_h = n^*a_1 + m^*a_2$ (noted as (n, m)). (n, m) is closely related to the electrical conductivity of CNTs. For a given (n, m) CNTs, the electrical conductivity of CNTs in this direction is the metallic if $2n + m = 3q$ (q is integer), and otherwise the performance is the semiconductor. For the condition of $n = m$, the electrical conductivity of CNTs is usually 10,000 times as much as that of copper.

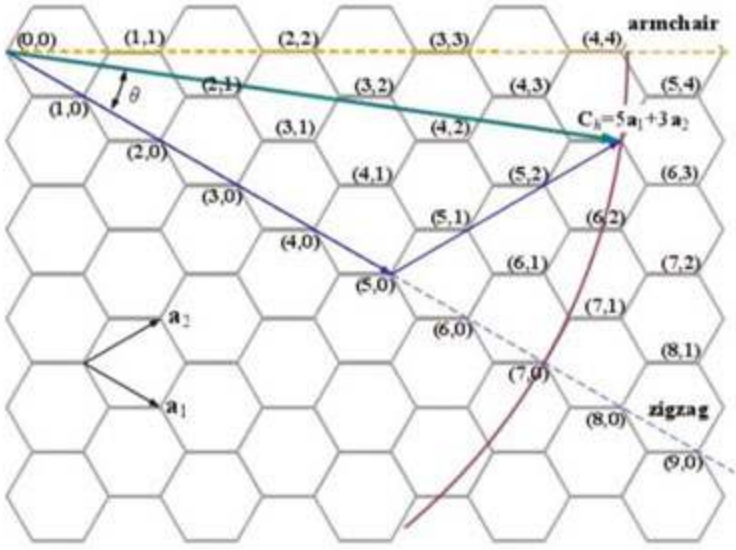

Figure 2. The Chiral vector selection of graphite flake.

1.1.5. The electron emission property of carbon nanotubes

CNTs have a nanometer scale point, which is benefit for to the electrons emission. Hence, scientists predicted and verified that CNTs have an excellent field emission effect.

1.1.6. The adsorption characteristics

CNTs have large surface activity and abundant pore structure. And the large surface area of the gas phase chemical composition has a strong adsorption and desorption capacity.

1.2. Carbon nanotubes preparation methods

1.2.1. Arc discharge method

It is the first and most used method to prepare CNTs. The main process is: (a) keep a certain pressure of inert gas or hydrogen in vacuum vessel, (b) choose graphite (with catalyst: nickel, cobalt and iron) as electrode. The graphite is consumed by evaporation at anode during the arc discharge process, and CNTs are received by depositing at cathode. Ebbesn et al [4]. successfully prepared gram order weight of CNTs under nitrogen gas condition, and then, this method is widely adopted. In 1994, Bethune introduced catalyst for arc reaction, reducing the reaction temperature and enhancing the productivity of CNTs. In 1997, Jounet et al. used catalysts for synthesizing single CNTs under helium condition. Sun Mingliang et al. studied the influence factors to CNTs prepared by DC arc discharge method: (a) inert gas pressure will affect the diameter and length of CNTs; (b) how much the adhesion of particles?; (c) oxygen and water vapor will lead to defects in CNTs, and it is unable to separate and purify after sintering together and (d) current and voltage will affect the yield and production rate of CNTs, but length to diameter ratio of graphite does not affect the generation of CNTs.

1.2.2. Catalytic cracking method

Catalytic cracking method, also known as chemical vapor deposition, prepares CNTs through cracking hydrocarbons or carbon oxides with the help of catalyst. The basic preparation process: (a) mixes the organic gases (such as acetylene and ethylene) with certain proportion of nitrogen gas in quartz tube. (b) CNTs grow on the surface of catalyst under certain temperature when the carbon source flow past and pyrolyze onto the surface of catalyst, and pushing forward the small catalyst particles [4]. (c) The growth of CNTs ends till all of the catalyst particles were coated with graphite layer. The advantages of the method are: easy to control the reaction process, simple equipment, low raw material cost, easy to produce the product in large scale, and the high productivity. The disadvantages are: too much CNTs layers, poor graphitization and exist crystalline defects. These disadvantages have great adverse influence on the physical and chemical properties of CNTs.

1.2.3. Laser evaporation method

Laser evaporation method prepares CNTs by illuminating the graphite target that contains metal catalyst. Then, the vapor mixes with carbon source and deposits on the surface of

substrate and the wall of reaction chamber. Smalley et al. received SWCNTs after adding a certain amount of catalyst to the electrode during preparing C_{60}. After improving the method, Thess et al. successfully fabricated amount of SWCNTs. Under the condition of 1473 K, the graphite target with Ni/Co catalyst particles was irradiated by double pulse laser with 50 ns, receiving the high-quality SWCNTs bundles.

1.2.4. Low-temperature solid-state pyrolysis method

Low-temperature solid-state pyrolysis prepares CNTs through intermediate. First, the nanometer level silicon nitride (Si_2C_2N) ceramic intermediate was prepared. The nanoceramic intermediate is then placed in a boron nitride crucible, which is heated in a graphite resistance furnace to decompose it with nitrogen gas as the protective gas. After 1 h, the nanointermediate powder begins to pyrolyze, and the carbon atoms migrate to the surface. A high proportion of CNTs are obtained with amount of silicon nitride powder in the surface pyrolysis products. The advantage of the low-temperature solid-state pyrolysis method is the repeatable production, which is beneficial for large-scale CNTs production.

1.2.5. Polymer pyrolysis method

The method prepares CNTs by decomposition of hydrocarbons precursor (such as acetylene and benzene) at high temperature. Cho et al. prepared CNTs by heating the polymer obtained from citric acid and glycol after polyesterification under 400°C for 8 h. The CNTs were synthesized by using metal Ni as catalyst in the temperature ranged from 420 to 450°C and under H_2 atmosphere. Under 900°C and Ar-H_2 atmospheric conditions, Sen et al. obtained CNTs by pyrolyzing ferrocene, nickelocene and cobaltocene. These metal compounds not only provide carbon source after pyrolysis, but also provide the catalyst particles. The growth mechanism of the method is similar to the catalytic cracking method.

1.2.6. Ion (electron beam) radiation method

In a vacuum furnace, carbon is evaporated by ion or electron discharge and deposit on the condenser. Chernazatonskii et al. synthesized CNTs with diameter range from 10 to 20 nm and high alignment by evaporating the graphite coated on the surface of substrates. Lin X et al. got CNTs with diameter range from 10 to 15 nm by irradiating amorphous carbon with argon ion beam under high vacuum environment [5].

1.2.7. Flame synthesis method

Flame synthesis method utilizes the heat, produced by burning methane and a small amount of oxygen, and imports hydrocarbons and catalysts at temperature of 600–1300°C to synthesize CNTs. The CNTs prepared by this method have the disadvantages of low crystallinity and large amount of amorphous carbon. There is still no definite explanation for the growth mechanism of CNTs nanostructure by flame method. Richter et al. found SWCNTs that attached with a large amount of amorphous carbon from carbon black after burning the mixture of acetylene, oxygen and argon gases. Daschowdhury et al. found nanometer tubular

CNTs by detecting carbon black after burning the mixture of benzene, acetylene, ethylene and oxygen gases.

1.2.8. Solar energy synthesis method

The CNTs are received from the condensation of high temperature (3000 K) mixture vapor of graphite and metal catalyst that heated by focusing the sunlight. This method is initially used for buckyballs production, then adopted for CNTs synthesis since 1996. Laplaze et al. synthesized the MWCNTs and SWCNTs use this method.

1.2.9. Electrolysis method

The preparation of CNTs by electrochemical method is a novel technique. This method adopts graphite electrode (electrolytic cell as anode), obtained carbon nanomaterials by electrolyzing molten alkali halide salts (such as LiCl) under a certain voltage and current with the protection of air or argon gases at about 600°C. The products include packaged or not packaged CNTs and carbon nanoparticles, and the form of carbon nanomaterials can be controlled by changing the process conditions of electrolysis. Andrei et al. found that CNTs can directly grow on the surface of n-type of (1 0 0) silicon electrode in solution of acetylene/ammonia. Hus et al. synthesized nanotubular and onion like CNTs under argon environment by using molten alkali metal halide as electrolyte and graphite as electrode. Huang Hui et al. successfully synthesized CNTs and carbon nanowires using LiCl and LiCl + $SnCl_2$ as molten salt electrolyte.

1.2.10. Other methods

Stevens et al. got CNTs by using an exothermic reaction between caesium and nanoporous amorphous carbon in the low temperature of 50°C. Chemozatonskii et al. found the fullerene and CNTs at the microholes of Fe_2Ni_2C, Ni_2Fe_2C and $Fe_2Ni_2Co_2C$ alloy prepared by powder metallurgy method [6]. Kyotani et al. first pyrolyze and deposit carbon on the wall of anodic alumina model (with nanometer trench) under 800°C. Then, hollow CNTs with open-end on both sides after removing the anodic alumina membrane by hydrofluoric acid can be obtained. Matveev et al synthesized CNTs using liquid nitrogen solution of acetylene at 233 K by electrochemical method. It is the lowest temperature ever reported to synthesize CNTs.

2. Modification CNTs

2.1. Simulation model build and computation method

This work chooses SWCNTs as a research object to present theoretical simulation for its adsorption of gas decomposition products of SF_6 and then explores its adsorption characteristics and predicts the detectable gas products. Materials Studio (MS) software developed by Accelrys Company is employed in this research, the $Dmol^3$ module of which is used for quantum mechanics stimulation. Generalized gradient approximation (GGA) approach, which

can accurately describe the geometric and electronic structures of CNTs as well as the processes of molecular interaction, is adopted to deal with the interchange and correlation between electrons, and its specific form is Perdew-Burke-Ernzerhof (PBE) [7]. The double-figure basis set (DNP) of polarization function is used in DFT (Density Functional Theory) calculation. In order to avoid the interactions between CNTs, a super grid 20 × 20 × 8.5 $Å^3$ has been designed, working under periodic boundary conditions. The initial distance between SWCNT and gas decomposition products of SF_6 is set as 0.16 nm. All atoms are calculated using full atomic potential, and the convergence value of self-consistent field is set as 10×10^{-5} eV/at [8]. Ref. [9] has shown that accurate results can be achieved by taking two K points in the (8, 0) SWCNTs Brillouin zone. All calculations above are accomplished on Dmol[3] module.

SWCNT, SF_6 as well as its gas decomposition products including SF_6, SO_2F_2, SOF_2, SO_2, H_2S, CF_4 and HF in the superlattices are optimized, respectively, to obtain the most stable structures before each calculation. **Figure 3** presents the stabilized configuration of SWCNT gas molecules (SF_6, SO_2F_2, SOF_2, SO_2, H_2S, CF_4 and HF) after geometrical optimization.

SF_6 and decomposition gas molecules are made to approach the C atom marked on the SWCNT in any possible posture, which is optimized to form a stable molecule-SWCNT system, respectively. Then, stable configurations will be found after a non-restrictive optimization to the molecule-SWCNT systems, and their electron properties will be calculated [8].

To assess the ability to interact between SWCNT and gas molecules, the adsorption energy E_b is calculated. E_b is defined as Eq. (1). E molecule-SWCNT-OH stands for the total energy of the molecule-SWCNT system after geometrical optimization, $E_{SWCNT\text{-}OH}$ and $E_{molecule}$, respectively, stand for the energy of SWCNT and that of an isolated molecule. If $E_b < 0$, it means the adsorption process is exothermic and can occur spontaneously.

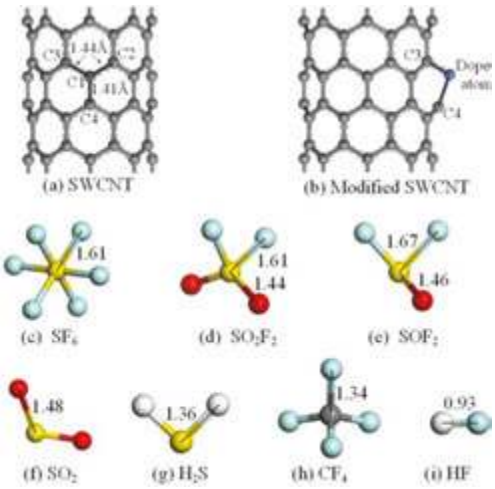

Figure 3. The most stable optimized configurations of SWCNT and gas molecules. The structural parameters are shown in Å. (a) SWCNT; (b) modified SWCNT; (c) SF_6; (d) SO_2F_2; (e) SOF_2; (f) SO_2; (g) H_2S; (h) CF_4; (i) HF.

$$E_b = E_{molecule-SWCNT} - E_{SWCNT} - E_{molecule} \quad (1)$$

The charge transfer Q_T between SWCNT and gas molecules is also computed to indicate the change of electrical conductivity of SWCNT, which can provide important information about electronic responses in the system [8]. The Q_T is calculated through the charge differences between the molecule adsorbed on the SWCNT and an isolated molecule itself as shown in Eq. (2) [8]:

$$Q_T = Q_{adsorped\ molecule} - Q_{isolate\ molecule} \quad (2)$$

Besides, the highest occupied molecular orbital (HOMO) energy level and lowest unoccupied molecular orbital (LUMO) energy level were studied to evaluate the energy needed for electrons to cross the energy barrier based on the frontier molecular orbital analysis [10, 11]. After the adsorption, the energy gap of the adsorption structure can be calculated through the energy levels of E_{HOMO} and E_{LUMO} defined as Eq. (3) [11].

$$E_g = \left| E_{LOMO} - E_{HOMO} \right| \quad (3)$$

2.2. Gas-sensing properties of intrinsic SWCNTs to SOF_2, SO_2F_2, SO_2, H_2S, HF, CF_4 and SF_6

2.2.1. Theoretical study: gas-sensing properties of intrinsic SWCNTs

2.2.1.1. The analysis of gas adsorption structure

We first studied the structure properties of pristine SWCNTs, Ni-SWCNTs, SO_2, SOF_2 and SO_2F_2. As an intrinsic structural beauty, SWCNTs consist of shells of sp^2-hybridized (trivalent) carbon atoms [12] forming a hexagonal network that is itself arranged helically within a tubular motif shown in **Figure 4a**. The bond lengths of zigzag bond C—C2 (C1—C3) and axial bond C1—C4 were 1.44 and 1.41 Å, respectively. **Figure 4** shows the most stable structures after gas molecules adsorb on the surface of intrinsic SWCNT. And the corresponding adsorption data are shown in **Table 1**.

It can be seen from **Figure 4**a, b and e and **Table 1**, the adsorption energy during the interaction of SF_6, HF and CF_4 with SWCNT is rather little, the adsorption energy of HF-SWCNT (−0.16 eV) is an order of magnitude lower than that of SF_6-SWCNT (−2.17 eV), and then, the adsorption energy of CF_4-SWCNT (−0.02 eV) is two orders of magnitude lower than that of SF_6-SWCNT; however, in terms of charge transfer, the number of charge transfer (0.038 au) between SWCNT and HF is an order of magnitude higher than that (0.005 au) between SWCNT and SF_6, while the number (0.003 au) between SWCNT and CF_4 is still lower than that, but in fact, the interacting distance is similar in the interaction of HF and CF_4 with SWCNT. As is shown above that SWCNT is insensitive to HF and CF_4 [8].

From **Figure 4c**, d and f and **Table 1** [8], it is clear that the adsorption energy during the interaction of H_2S, SO_2 and SOF_2 with SWCNT is almost in the same level; the number of charge transfer between SWCNT and H_2S (0.008 au) is a bit higher than that between SWCNT and SF_6 (0.005 au); however, they are in the same order of magnitude, while the number of charge

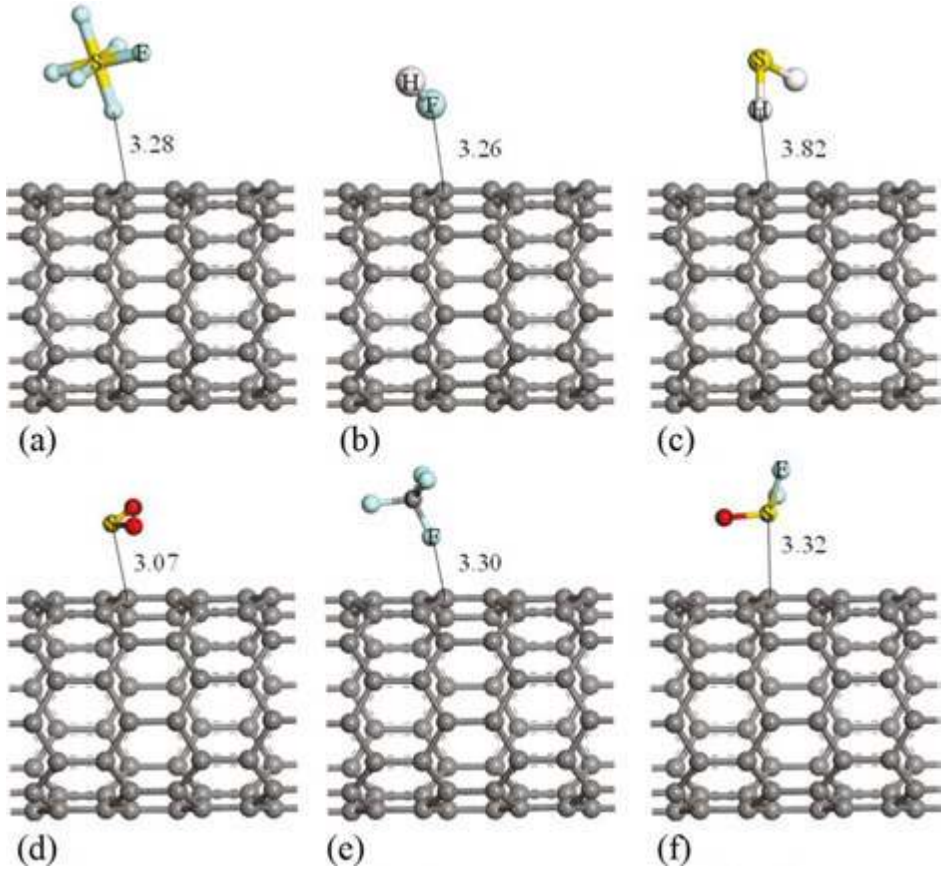

Figure 4. The most stable optimized configurations of gas molecules interacting with SWCNT, respectively. The structural parameters are shown in Å. (a) SF_6-SWCNTs; (b) HF-SWCNTs; (c) H_2S-SWCNTs; (d) SO_2-SWCNTs; (e) CF_4-SWCNTs; (f) SOF_2-SWCNTs.

System	Figure	E_b (eV)	Q_T (au)	D (nm)
SF_6-SWCNT	3a	−2.17	0.005	0.3278
HF-SWCNT	3b	−0.16	0.038	0.3262
H_2S-SWCNT	3c	−2.17	0.008	0.2822
SO_2-SWCNT	3d	−2.23	0.054	0.3071
CF_4-SWCNT	3e	−0.02	0.003	0.3299
SOF_2-SWCNT	3f	−2.21	0.017	0.3320
SO_2F_2-SWCNT	4a, b	−1.19	0.403	0.1943

Table 1. Calculated adsorption energy, charge transfer and interacting distance.

transfer between SWCNT and SO_2, SOF_2 is an order of magnitude higher than that between SWCNT and SF_6. But the interacting distance is similar in the interaction of SO_2, SOF_2, SF_6 with SWCNT. It means the sensitivity of SWCNT to H_2S, SO_2 and SOF_2 is the same as that to SF_6, so there is cross-sensitivity between them. Under the background of the high concentration of SF_6, SWCNT as a gas sensor is unable to accurately detect H_2S, SO_2 and SOF_2.

Figure 5 presents the most stable configurations of SO_2F_2-SWCNT. **Figure 5a** presents the chart whose chemical bond is not displayed; **Figure 5b** gives the chart whose chemical bond is displayed by MS. From **Figure 5b**, it is seen that the S atom in SO_2F_2 has formed the bond with the C atom marked in SWCNT, and the F atom has formed the bond with adjacent C atom yet, which means that the chemisorption between SWCNT and SO_2F_2 occurs. It can be inferred based on the data above that the adsorption energy of SO_2F_2-SWCNT is lower 0.98 eV than that of SF_6-SWCNT, but they are in the same order of magnitude, which shows that there exist differences between them. However, the number of charge transfer (0.403 au) between SWCNT and SO_2F_2 is 80 times higher than that (0.005 au) between SWCNT and SF_6, which shows that the conductivity of SWCNT has changed a lot after adsorbing SO_2F_2. The interacting distance during the interaction of SO_2F_2 with SWCNT is obviously less than that of other molecules. Therefore, it can be concluded that SWCNT is the most sensitive to SO_2F_2 in all the gas decomposition products of SF_6.

2.2.1.2. The analysis of the density of states

From **Figure 6**, it is clear that the density of states curves of SWCNT almost coincides after adsorbing HF, H_2S and CF_4 [8], which reveals that the electronic structures and conductive properties of SWCNT are basically unchanged, so SWCNT is not sensitive to HF, H_2S, and CF_4. However, the density of states curves shifts to the right of Fermi level after SOF_2 and SO_2 are absorbed, which indicates that the electronic structures are changed. There is a short overlap of DOSs between SWCNT and SO_2-SWCNT near Femi level, so the conductive properties change a little. But the DOSs peak of SOF_2-SWCNT is lower than that of SWCNT in the

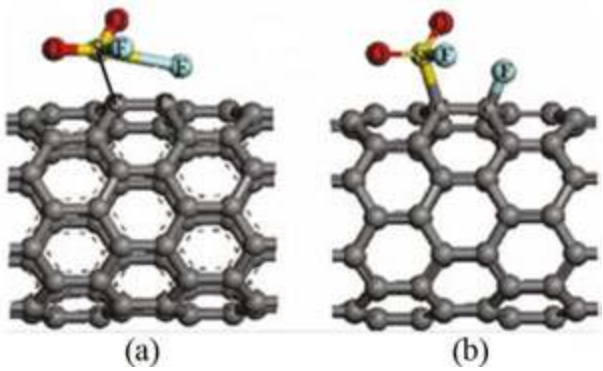

Figure 5. Optimized the most stable configurations of SO_2F_2-SWCNT. (a) Bonds not displayed by MS; (b) bonds displayed by MS.

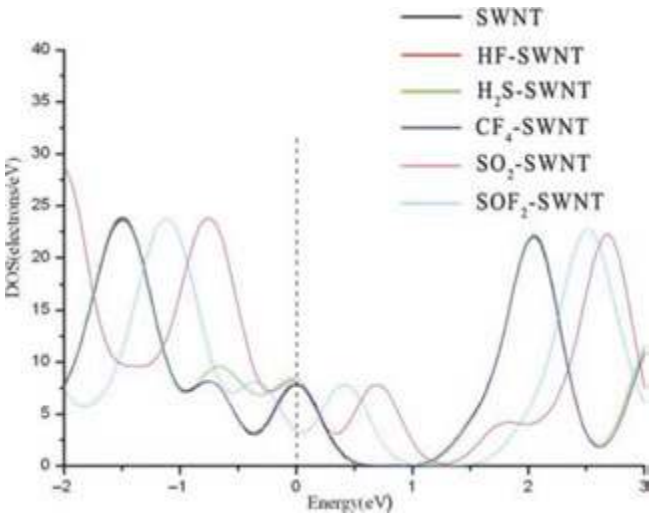

Figure 6. The DOSs of molecules-SWCNT. Dotted line indicates the Fermi level.

Fermi energy level, which means that the number of quantum states occupied by electrons in the Fermi energy level has reduced when SOF_2 molecules adsorbed on SWCNT, causing SWCNT's conductivity decreased. Finally, it can be concluded that the sensitivity of SWCNT to SO_2 is similar to SOF_2 [8].

From the **Figure 7**, it can be derived that DOSs has changed a lot after absorbing SF_6, SO_2F_2 in and near the Fermi level. DOSs curve of SO_2F_2-SWCNT is higher than SWCNT's, while

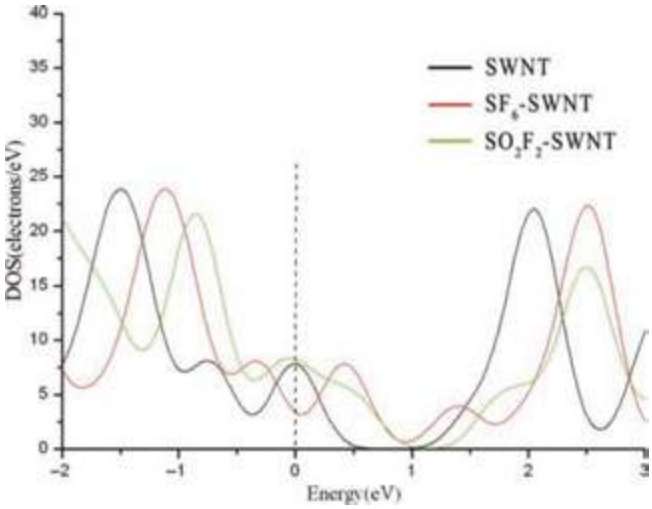

Figure 7. The DOSs of SWCNT, SF_6-SWCNT and SO_2F_2-SWCNT. Dotted line indicates the Fermi level.

DOSs curve of SF_6-SWCNT is lower than SWCNT's. The number of quantum states occupied by electrons near the Fermi energy level has increased after SO_2F_2 adsorbed by SWCNT, the properties of SWCNT becoming more active and conductivity being enhanced, on the contrary, the properties of SWCNT become less active after absorbing SF_6. Based on the analysis above, SWCNT is the most sensitive to SO_2F_2.

Band structures of SWCNT, SF_6-SWCNT and SO_2F_2-SWCNT are given in **Figure 8a–c**, from which we can see that the energy gap (Eg1 of SWCNT is about 0.022 ha (0.60 eV),

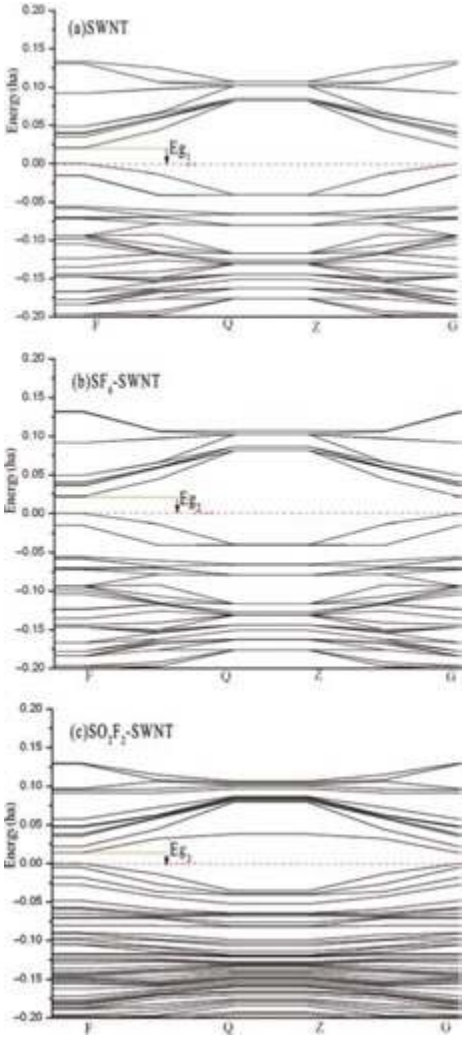

Figure 8. The band structure diagrams of (a) SWCNT, (b) SF_6-SWCNT and (c) SO_2F_2-SWCNT. Dotted line indicates the Fermi level.

SF_6-SWCNT (Eg2 is about 0.022 ha (0.60 eV) and SO_2F_2-SWCNT (Eg3) is about 0.015 ha (0.40 eV), which reveals that the conductivity is unchanged after absorbing SF_6, but the conductivity is increased after absorbing SO_2F_2. Thus, it can be predicted that SWCNT can serve as gas sensors to detect SO_2F_2, one of the decomposing gas products of SF_6, in partial density (PD).

2.2.2. Experimental study: gas-sensing properties of intrinsic SWCNTs

2.2.2.1. Preparation of plasma-modified intrinsic SWCNTs

MWCNTs (tube diameter, 20 to 30 nm; length, 10 to 30 μm; purity, >95%) were grown by chemical vapor deposition (CVD) in black powder and purchased from the Chengdu Institute of Organic Chemistry Chengdu, China. CNTs are one-dimensional (1D) nanomaterials. Hence, appropriate surface processing parameters should be selected. Under strong plasma treatments, high power and long treatment time can destroy the tubular structure and carbonization of CNTs [13, 14]. In this study, a DBD plasma generator was used to modify MWCNTs. **Figure 9** shows the schematic for the test device. Low-temperature plasma experimental power (CTP-2000K) used in this experiment was produced from Nanjing Rongman Electronics Co., Ltd., China. The input voltage of the experimental power is controlled by a voltage regulator. Adjust the voltage to 30 V, which can be reading from the Voltmeter (Power input) in the power device. Adjust output frequency knob in the experimental power until frequency is around 10 kHz. Then, we can get an optimum DBD discharge. Read the input current of 1.96 A from Ammeter in the power device. Using oscilloscope to obtain the output voltage and current waves, and displayed in **Figure 9**. We should point out that there is an attenuator in this experimental power, and the attenuation coefficient is 1000. So the output peak-to-peak voltage is 39.3 kV. The discharge power in DBD plasma reactor can be calculated by Lissajou curve. However, due to the poor laboratory conditions, we do not have enough oscilloscope attenuation probes to protect oscilloscope from breakdown. So other method should be explored, and we try to get in touch with the equipments manufacturers. According to the experience of the manufacturer's data, the plasma treatment power is approximately 0.8 times of the input power at the same experimental conditions. Therefore, we can calculate the discharge power which is 47 W.

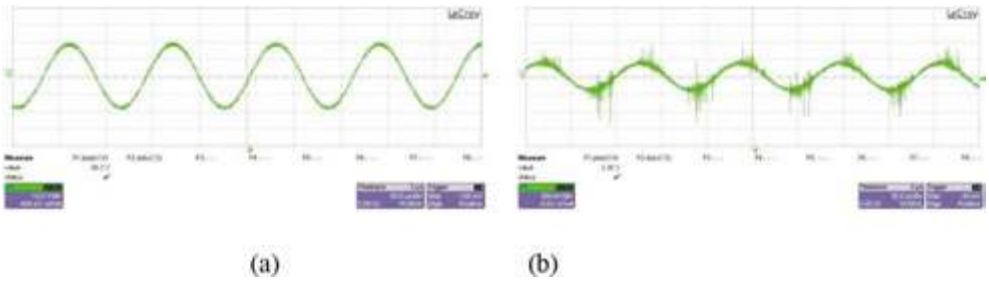

Figure 9. Discharge waveforms (a) output voltage waveform and (b) output current waveform.

Figure 10 reveals that the shape of the reactor is similar to a Petri dish. The reactor electrodes formed a parallel-plate structure and were made of 2-mm thick quartz glass. The upper and bottom electrodes were 8 mm apart. The bottom quartz glass electrode adhered to the reaction kettle, whereas the upper electrode is removable. In the modified experiment, an adequate amount of MWCNTs was placed in a reaction kettle and sealed with silicone to ensure gas tightness. Air was released from the reactor to induce a vacuum state. CF_4 flow rate was controlled at 150 sccm. The parameters of the experimental power were adjusted, and MWCNTs were, respectively, treated for 0.5, 1, 2, 5, 8, 10 and 12 min. The upper quartz glass was removed, and modified MWCNTs were obtained after the treatment.

2.2.2.2. Preparation of plasma-modified MWCNTs-based sensors

MWNT sensors were made of printed circuit board, and the substrate material is epoxy resin. Cu interdigital electrodes were etched in the substrate. The width and spacing of the electrodes are both 0.2 mm. First, MWCNTs were placed into a beaker containing the appropriate ethanol solution. The beaker was placed in an ultrasonic bath for 1 h. Then, the sensor substrate was repeatedly cleaned with deionized water to remove impurities on the electrode surface. Next, the mixed solution was dropped on the substrate surface. Finally, the MWNT-coated substrates were baked in an oven at 80°C for a specific time. This process was repeated several times until uniform MWCNTs films were deposited on the surface. Seven pristine and treated MWCNTs with different modification times were used to fabricate the gas sensors.

2.2.2.3. Characterization of plasma-modified MWCNTs

FTIR spectra are highly useful tools to analyze the characteristics of CNTs. **Figure 11** shows the FTIR spectra of pristine MWCNTs and those generated by CF_4 plasma etching for 1, 5 and 10 min with a Nicolet 5DXCFT-IR spectrometer.

Diverse functional groups and types of bonding were observed in the FTIR spectra of MWCNTs (**Figure 11**). The absorption peaks at 3445 cm^{-1} corresponded to the ─OH groups in pristine and treated nanotubes. The absorption peaks at 1036 and 1151 cm^{-1} were ascribed to the respective C─F and symmetric ─CF_2 stretching vibrations because of the CF_4 plasma treatment.

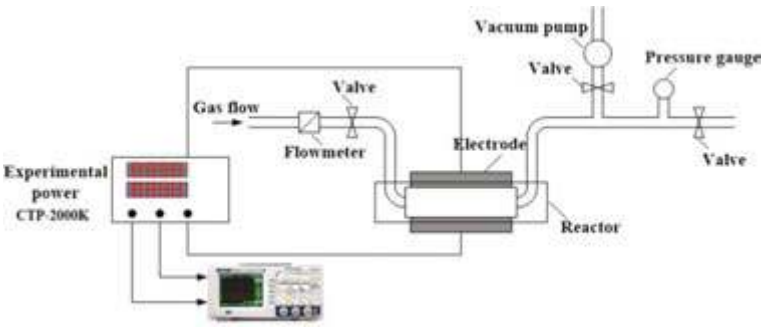

Figure 10. Schematic of the DBD experiment setup.

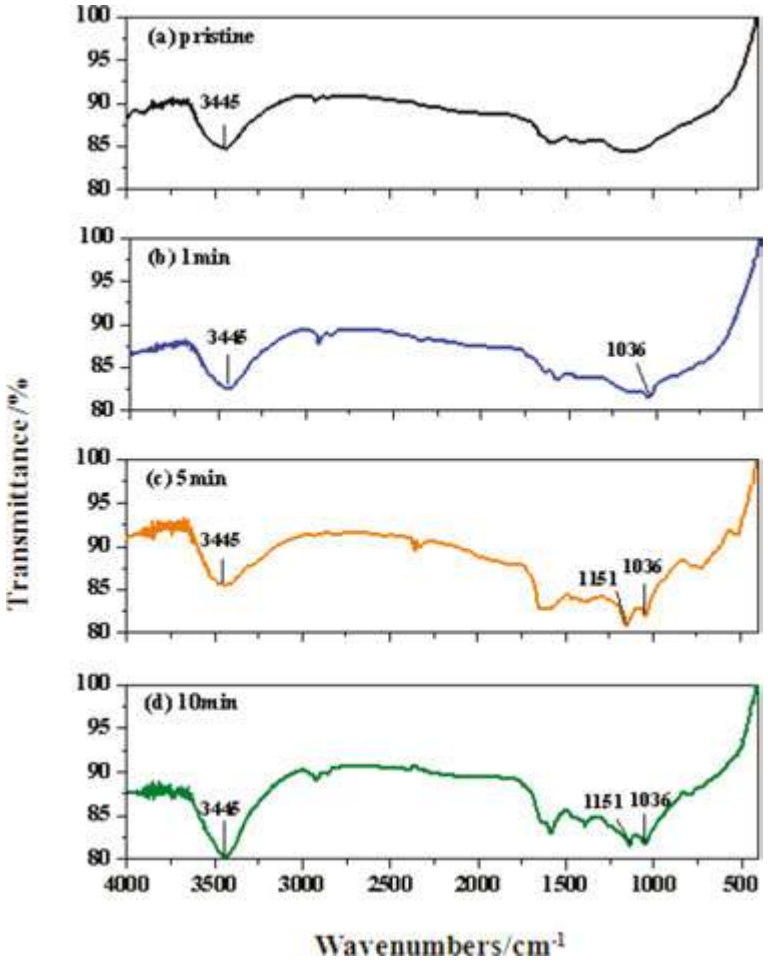

Figure 11. Infrared spectra of pristine and modified MWCNTs. (a) Pristine; (b) 1 min; (c) 5 min; (d) 10 min.

The surface morphologies of the pristine and plasma-treated MWCNTs were analyzed using Zeiss Auriga focused ion beam and double-beam emission scanning electron microscopy (SEM). The SEM images of pristine MWCNTs (**Figure 12a**) indicated the presence of several small particles, which included amorphous carbons and residual catalysts during preparation. **Figure 12b** and **c** shows the SEM images of CF_4 plasma treated for 10 min. The impurities and dopant on the nanotubes surfaces were removed, and MWCNTs became shorter. Plasma treatment retained the nanotubes structures.

2.2.2.4. The analysis of the gas-sensing properties

We used eight kinds of MWCNTs-based gas sensors (pristine MWCNTs and MWCNTs modified by plasma for different time) to detect H_2S and SO_2 whose concentration is both

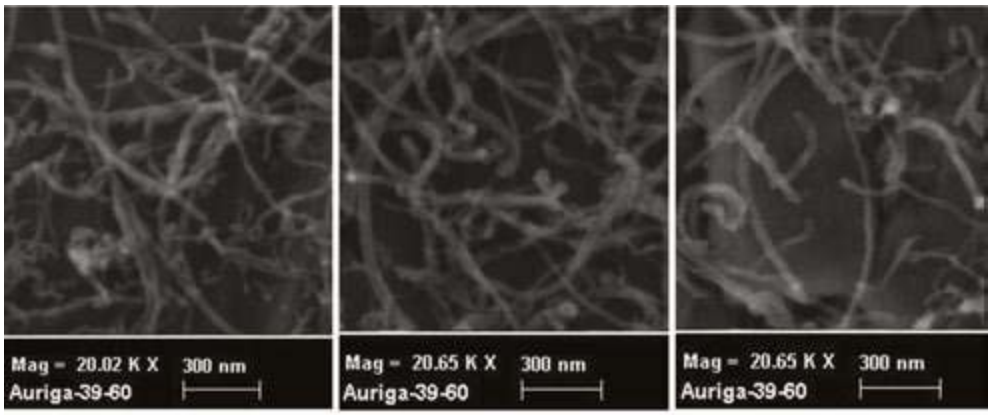

Figure 12. SEM images (a) pristine and (b and c) modified MWCNTs for 10 min.

50 ppm. The gas response curves are shown in **Figure 13**. It can be seen from **Figure 13a** and b that the sensitivity of pristine MWCNTs and those modified by CF_4 plasma for 0.5, 1 and 2 min to H_2S are 3, 3.2, 3.4 and 3.5%, respectively, and to SO_2 are 2.3, 2.4, 2.6 and 2.7%. Obviously, after modification, the gas sensitivities of MWCNTs are not markedly enhanced. Under small discharge power, these phenomena may have been caused by the insufficient treatment time and poorly surface modification. Therefore, if the discharge power remains unchanged, in order to achieve a better surface modification, plasma treatment time should be extended.

In consequence, **Figure 13c** and **d** shows the response curves of pristine MWCNTs and these treated for 5, 8, 10 and 12 min to H_2S and SO_2. We can see that when the treatment time is less than 10 min, the sensitivities of MWCNTs sensors increased with increasing of treatment time. Meanwhile, the MWCNTs modified by CF_4 plasma for 10 min exhibited the best sensitivity both to H_2S and SO_2. However, the sensitivities decreased when the treatment time is over 10 min. Possible reasons may be that after longer treatment time, the structure of the nanotubes was destroyed, and nanotubes were partly carbonized [13] under the bombardment of energetic particles in prolonged plasma treatments, which result in a reduce of active adsorption sites on MWCNTs surface for gas molecules. Hence, the gas-sensing properties of the MWCNTs were affected.

Figure 13 reveals that the response time of CF_4 plasma-modified MWCNTs sensors to H_2S and SO_2 was shorter. For treatment times ranging from 0 to 10 min, the response time decreased with increasing treatment time. Besides, the shortest response times to H_2S and SO_2 are 70 and 150 s, respectively.

Responses of MWCNTs-based sensors to H_2S and SO_2 at different concentrations are studied in this work. MWNT sensors modified by CF_4 plasma for 10 min (Section 3.3) were selected to

http://dx.doi.org/10.5772/intechopen.68325

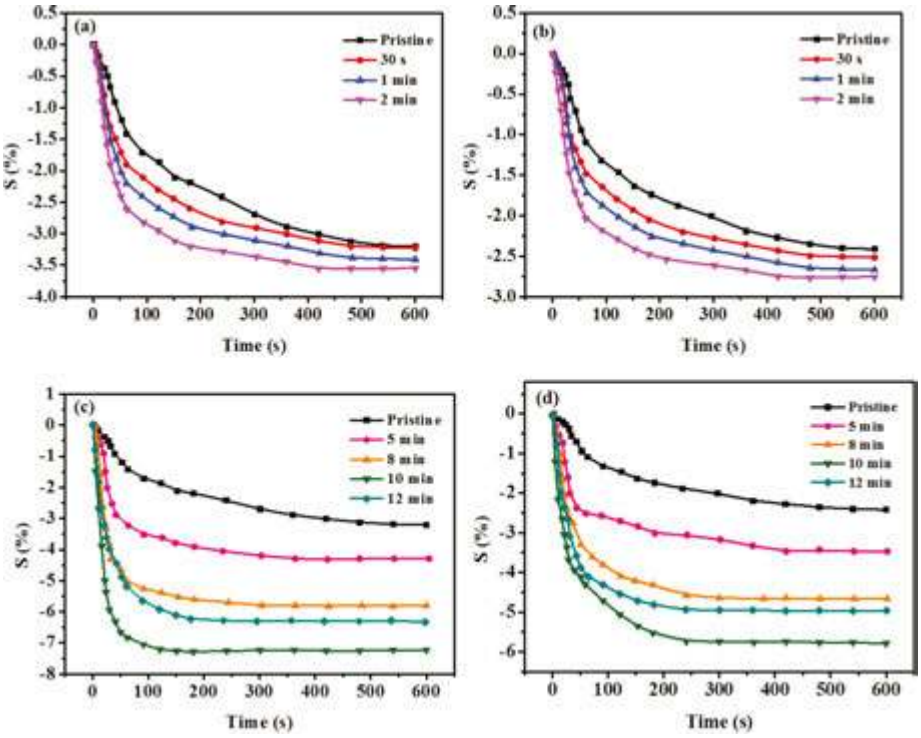

Figure 13. Responses of MWCNTs-based gas sensors (a, c) 50 ppm H_2S and (b, d) 50 ppm SO_2.

detect H_2S and SO_2 at 10, 25, 50 and 100 ppm because these sensors yielded the best sensitivities. **Figure 14a** and **b** indicates that the sensitivity of the sensors increases with the gas concentration.

Figure 15 shows that the gas concentration and sensor sensitivity were linearly correlated for H_2S and SO_2 concentrations of 10–100 ppm with correlation coefficients (R^2) of 0.97183 and 0.9739, respectively.

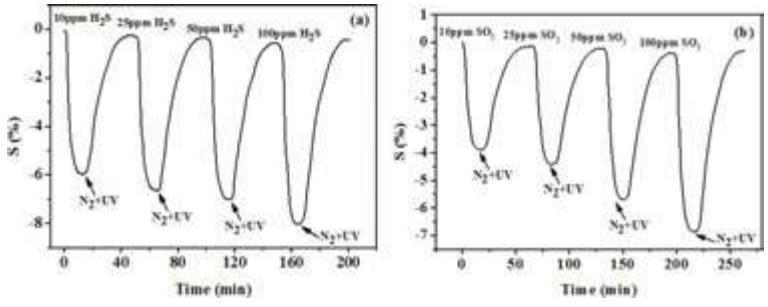

Figure 14. Response curves of MWCNTs-based sensors to different concentrations of (a) H_2S and (b) SO_2.

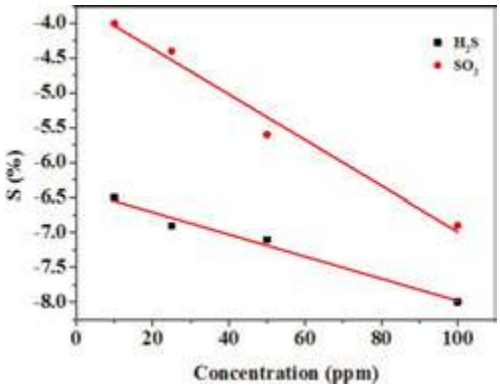

Figure 15. Linear relationship sensitivity of MWNT-based sensors for different concentrations of SO_2 and H_2S.

2.2.2.5. Desorption and repeatability of MWCNTs-based sensors

To analyze the desorption properties of modified MWCNTs gas sensors, these modified by CF_4 plasma for 10 min were chosen to test the recovery curve, as shown in **Figure 16**. The experiment steps are as follows. Firstly, the chamber was pumped into vacuum and standing for a period of time. After resistance of the sensor remains unchanged, in the second minute 50 ppm, H_2S was introduced into the chamber, and the resistance showed a quick decrease. Few minutes later, the resistance of sensor remains stable. Currently, H_2S gas molecules reach adsorption equilibrium at the surface of MWCNTs. In the fifth minute, pure N_2 was injected into the gas chamber, and the sensor resistance can generally recover near the initial value. There still have a small amount of residual gas accumulates on the surface of the sensor which affect the sensitivity. In order to obtain a completely desorption, placed the sensor under UV irradiation. By irradiating with UV light, the residual gas absorbs energy, which enables it to

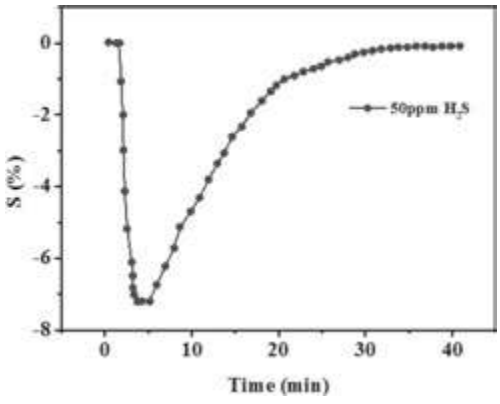

Figure 16. Recovery curve of plasma-modified MWCNTs to H_2S.

"escape" from the "trapped" state where almost no residual gas remains on the surface of the tested sensor. After N_2 and UV treatments, the sensor resistance was gradually restored to its initial value. The recovery time was about 25 min, which was less than that of the pristine MWCNTs sensor to H_2S (40 min; data not shown).

The MWCNTs sensor modified by plasma for 10 min that was most sensitive to SO_2 was selected to illustrate the repeatability process (**Figure 17**). The resistance-change trends remained similar, and the maximum resistance-change rate remained the same and stable. Hence, the gas sensor could be repeatedly used with good response and stability. However, the recovery time was approximately 35 min and was not greatly enhanced in contrast to that of pristine MWNT-based sensors.

2.2.2.6. Gas-sensing mechanism

The CF_4 plasma-modified MWCNTs sensors exhibited high sensitivities to H_2S and SO_2 because of the following reasons: (1) The accelerated electrons, ions and free radicals cleaned the MWNT surface by etching some amorphous carbon and catalyst particles during plasma treatment; (2) the bombardment of energetic particles destroyed some of the nanotubes and increased the defects on their surfaces, which generated effective adsorption sites for gas molecules; and (3) CF_4, a fluorinated gas [14], was ionized to generate fluoride ions in DBD and react with carbon atoms on the MWCNTs surface to yield C—F bonds [15] without destroying the tubular structure. Given the strong polarity and reactivity of F atoms, fluorinated MWCNTs exhibited strong adsorption capacities and high gas-sensing properties.

The response and recovery time of plasma-modified MWNT sensors to H_2S were remarkably reduced, but only the response time to SO_2 decreased, and recovery time was not reduced (Section 3.5). Theoretically, H_2S molecules were physically adsorbed on the surface of MWCNTs through van der Waals interaction. However, some hydroxyls existed on the surfaces of the nanotubes during growth by CVD. F atoms were introduced onto the MWCNTs

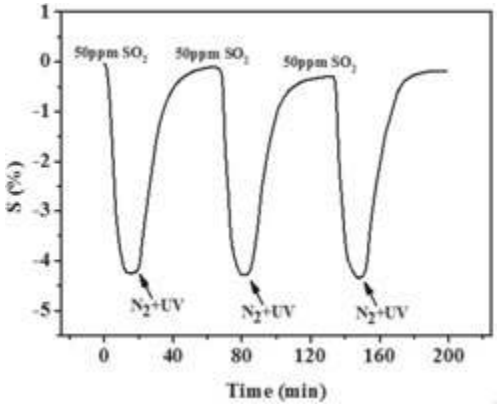

Figure 17. Reversibility curve of modified MWCNTs to 50 ppm SO_2.

surface after fluorination. C—F bonds possessed high polarity because of the strong electro negativity of the F atom, during which —F was essential. Stable hydrogen bonds (C—F… H—S) were formed between H atoms in H_2S molecules and F atoms when H_2S molecules were adsorbed on the surface of modified MWCNTs. Subsequently, the van der Waals forces were replaced, and the adsorption of H_2S molecules was accelerated to reduce the response time (**Figure 18a**). In addition, O atoms in the hydroxyl groups in MWCNTs surfaces exhibited small atomic radii and high electro negativities. Hydrogen bonds (C—O…H—S) were formed between O atoms in hydroxyl and H atoms in H_2S molecules (**Figure 18a**). The recovery time of plasma-based MWCNTs sensors to H_2S decreased possibly because of the effect of UV irradiation that the H—F bond is easier to disintegrate. For SO_2, only O atoms in the SO_2 molecules and H atoms of hydroxyl were combined to form hydrogen bonds [O—H…O—S; **Figure 18b**]. F atoms on the surfaces of modified MWNT increased the number of effective adsorption sites for gas molecules, accelerated the adsorption and reduced the response time. However, the recovery time remained invariant.

2.2.3. Summary: gas adsorption on intrinsic SWCNT

In the theoretical study aspect, the adsorption between SWCNT and SO_2F2 was chemisorption because new covalent bonds were formed. The number of charge transfer between SWCNT and SO_2F_2 was 80 times higher than that of between SWCNT and SF_6, and also higher than that of other gas decomposition products, which show that the adsorption is the strongest. The calculated DOSs indicated that the SO_2F_2 gas molecules adsorbed on SWCNT had changed the electronic structures of SWCNT, chemical properties of SWCNT becoming more active. In fact, the conductivity of SWCNT was also enhanced because the energy gap of SWCNT had decreased from 0.022 ha (0.60 eV) to 0.015 ha (0.40 eV) when the SO_2F_2 gas molecules were adsorbed. However, HF, H_2S and CF_4 molecules adsorbed on SWCNT had little effect on the electronic structures of SWCNT, so SWCNT's properties kept unchanged. Due to the cross-sensitivity of SWCNT to SF_6, SO_2 and SOF_2 molecules, SWCNT cannot detect the SO_2 and SOF_2, respectively. Thus, based on the analysis above, SWCNT can be prepared a gas sensor to detect SO_2F_2 gas among the gas decomposition products of SF_6 in PD.

In the experimental study aspect, MWCNTs grown by the CVD method are initially modified by atmospheric pressure DBD air plasma and are used as gas-sensitive materials. Then,

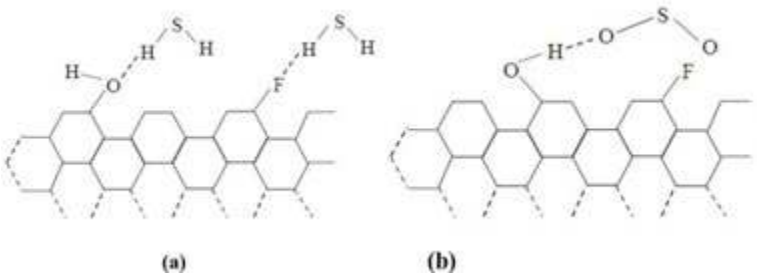

Figure 18. Schematic of the absorption of (a) H_2S and (b) SO_2 in modified MWCNTs.

the gas sensitivity of the unmodified and modified MWCNTs to 50 ppm H_2S and 50 ppm SO_2 is tested, respectively. The results show that the sensitivity of modified MWCNTs to H_2S is enhanced 2.75 times, and the response time to H_2S greatly reduced [16]. However, the sensitivity of modified MWCNTs to SO_2 exhibits the opposite effect. The MWCNTs are almost no longer sensitive to SO_2. Thus, the MWCNTs modified by atmospheric pressure DBD air plasma presented good selectivity to H_2S and have great potential value in the detection of this gas [16].

2.3. Gas-sensing properties of Pd-SWCNTs to SOF_2, SO_2F_2, SO_2, H_2S, HF, CF_4 and SF_6

2.3.1. Structural parameters of intrinsic Pd-SWCNTs

The geometric structure of the SWCNTs is dramatically distorted after substitution as shown in **Figure 19**. The impurity of the Pd atom induces the deformation of the six-membered ring near the doping site to relieve stress, which results in the carbon site substituted by the Pd heteroatom that evidently protrudes out of the tube wall because the radii of the Pd atom are larger than other carbon atoms [17, 18].

2.3.2. The analysis of gas adsorption structure

The SO_2, H_2S, SOF_2, SO_2F_2 and CF_4 gas molecules were made to approach the Pd atom marked on the SWCNTs at any possible posture to find the most stable adsorption system (see **Figure 20**). The adsorption energy E_{ads}, Q_T and interactive distance d are computed to analyze gas response property. All the parameters and configurations are shown in **Table 2** and **Figure 20**, respectively. From **Table 2**, we found that the adsorption energy of all the molecules is negative, so the adsorption reaction is an exothermic process that occurs spontaneously.

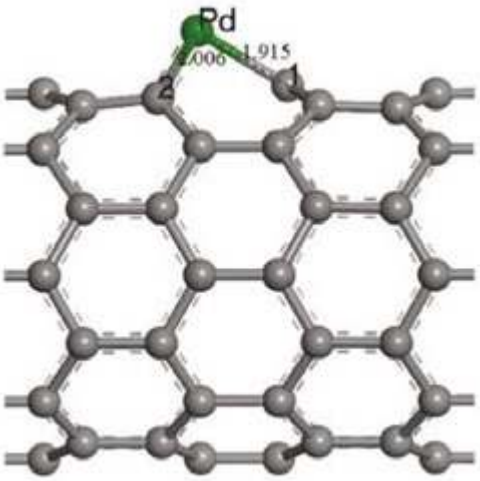

Figure 19. Geometric structures of Pd-doped SWCNTs after optimization. The structural parameters are shown as Å.

Pd acts as the adsorption site in the process of SO_2 adsorption. When one SO_2 molecule approaches the Pd atom and the adsorption structure is optimized to find the steady state (**Figure 20a1**), the two oxygen atoms labeled O1 and O2 are seen close to the Pd atom, whereas the S atom is seen away from the Pd atom, indicating that the Pd and O atoms form a coordinate bond, and the interaction between the Pd and S atoms is weak. The interatomic distance S—O1 changes from 1.480 to 1.565 Å, and the Pd-O1 distance is 2.281 Å in the reaction process, indicating that SO_2 adsorbed on the surface results in the elongation of the S—O bond. The result is agreement with our previous study [19], where the interaction distance between the Pd atom and the SO_2 in our present Pd-doped (8, 0) SWCNTs is generally slightly smaller than that of Pd-doped (5, 5) SWCNTs [20]. The long molecule surface distance 2.281 Å and low banding energy −0.798 eV suggest some kind of physisorption. Upon the adsorption of the second SO_2 molecule on Pd-SWCNTs (**Figure 20a2**), the two molecules become simultaneously close to the Pd atom through the oxygen atom O1' and O2'. The adsorption distance of Pd-O1' and Pd-O2' is 2.231 and 2.236 Å, respectively, which shows no distinct difference to that of single SO_2 adsorption, whereas the interatomic distance of SO_2 becomes slightly elongated compared with the individual molecule causing increased bonding strength between the Pd atom, O1', and O2'.

The optimized structures of H_2S adsorbed on Pd-SWCNTs are shown in **Figure 20b1** and**b2**. The interaction between H atoms of H_2S and Pd is too weak, and thus, adsorption of H_2S through S atom is an appropriate adsorption conformation course for the multiple valence states of the S atom. Upon single molecule adsorption, a quasi-tetrahedron geometry around the Pd center with H_2S forms in one of the apical positions upon adsorption of H_2S. The Pd-S long distance 2.570 Å and the low banding energy −0.802 eV are received in the process of adsorption, which suggests that H_2S undergoes moderate physisorption. After the second H_2S approached the Pd-SWCNTs, both H_2S molecules were situated around the Pd atom in a similar geometrical morphology. The results showed that Pd-SWCNTs had similar adsorption ability with both of the H_2S molecules. The total adsorption energy of the two H_2S molecules has reached −1.361 eV with Pd-S1' and Pd-S2' distance of 2.689 and 2.588 Å, respectively. The adsorption energy has been much enhanced than our previous studied gold doped (8, 0) SWCNT [21]. The H_2S molecules act as electron donor, and the charge transfer QT is 0.481 e. The large adsorption energy and considerable charge transfer made the Pd-SWCNTs a possible sensor material to detect H_2S. Star et al. reported that Pd-Decorated CNTs show good response to 50 ppm H_2S using the experimental method [22].

The adsorption of SOF_2 on the surface of Pd-doped (8, 0) SWCNTs is more stable from the F atom toward the Pd site, as shown in **Figure 20c1** and **c2**. The calculated binding energy for the SOF_2 interacted across the Pd atom of (8, 0) SWCNTs is −0.846 eV, and the adsorption distance between the F1 atom of molecule and the Pd atom of tubes is 2.003 Å, whereas the distance between F1-S bond increased to 2.778 Å. The large binding energy and structure change shown by the SOF_2 molecule presents a strong chemical interaction with the Pd-doped SWCNTs [23]. The Mulliken population analysis showed that the SOF_2 adsorption on Pd-doped (8, 0) SWCNTs leads to 0.572 electron transfer from the tubes to the SOF_2 molecule. Therefore, SOF_2 functions as an electron acceptor, whereas the nanotube functions as an electron donor. From **Figure 20c2**, we found that the adsorption distance between the second SOF_2 and the Pd-SWCNTs was 4.649 Å. Therefore, the adsorption is obviously weaker than

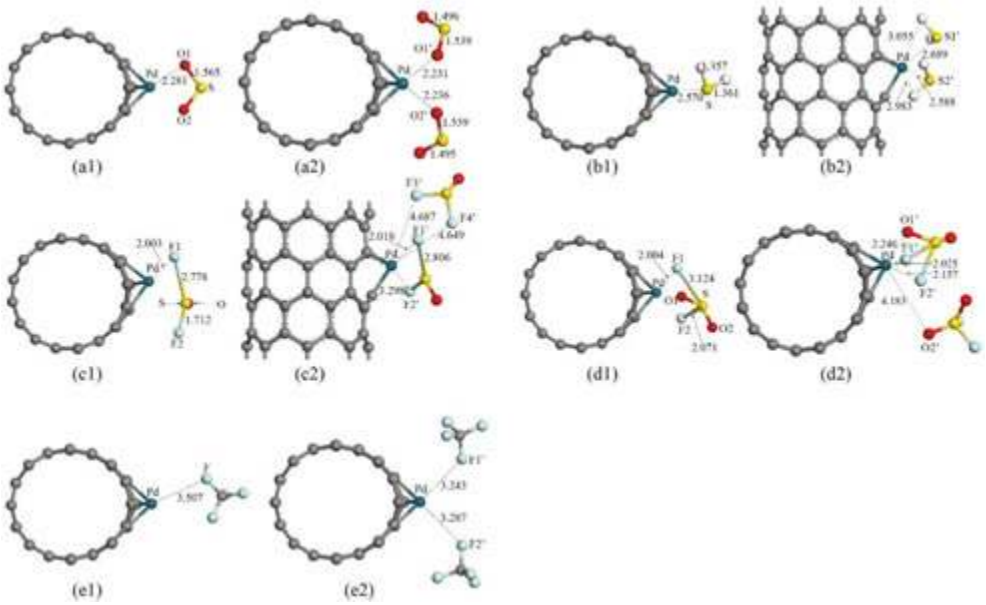

Figure 20. The most stable optimized geometries of gas molecules interacting with Pd-doped SWCNTs. The structural parameters are shown in Å.

the first adsorbed Pd-SWCNTs. The increased adsorption energy induced by the second SOF_2 is only −0.178 eV, which has also confirmed the weak interaction between the second SOF_2 molecule and Pd-SWCNTs. To some extent, the result can be attributed to the strong repulsive force between the SOF_2 molecules. Meanwhile, the charge transfer Q_T is only −0.604 e, which is only 0.032 higher than that of single SOF_2 adsorption.

System	Structure	E_{ads} (eV)	Q_T (e)	d_1 (Å)	d_2 (Å)
SO_2	(a1)	−0.798	−0.304	2.281	/
$2SO_2$	(a2)	−1.120	−0.368	2.231	2.236
H_2S	(b1)	−0.802	0.278	2.570	/
$2H_2S$	(b2)	−1.361	0.481	2.689	2.588
SOF_2	(c1)	−0.846	−0.572	2.003	/
$2SOF_2$	(c2)	−1.024	−0.604	2.018	4.649
SO_2F_2	(d1)	−1.627	−0.991	2.004	/
$2SO_2F_2$	(d2)	−1.735	−0.973	2.025	4.183
CF_4	(e1)	−0.046	−0.001	3.507	/
$2CF_4$	(e2)	−0.097	0.009	3.243	3.287

Table 2. Calculated adsorption energy, charge transfer and the binding distance from Pd atom to the adsorbates.

In the adsorption of SO_2F_2 (**Figure 20d1** and **d2**), although the adsorption energy value of single SO_2F_2 molecule is in the same order of magnitude as SO_2 and SOF_2, the adsorption energy of SO_2F_2 (−1.627 eV) is still almost twice over SO_2 (−0.798 eV), SOF_2 (−0.846 eV), and even reached 20 times more that the value of CF_4 (−0.086 eV). The interatomic distance S-F1 increased from 1.611 to 3.124 Å with an S-Pd distance of 2.004 Å. Therefore, we concluded that Pd doping makes the SWCNTs preferable for SO_2F_2 chemisorption. The adsorption of two SO_2F_2 is similar to SOF_2, which is the first SO_2F_2 near the Pd atom with a binding distance of −2.025 Å. The second molecule from the Pd atom with a distance of 4.183 Å creates the repulsive force between the SO_2F_2 molecules. The total adsorption energy is Pd atom 1.735 eV, and the charge transfer is −0.973 electron, which are almost the same with the values of single SO_2F_2 adsorption.

The adsorption of CF_4 (**Figure 20e1** and **e2**) is only −0.046 eV because of weak van der Waals interaction between two species, and nearly no charge transfer was present [24]. The energy is the least one among all gas molecules adsorption. The interacting distance from Pd atom to the atom F1 is 3.507 Å. Upon the two molecules' adsorption, the Pd-F1' and Pd-F2' are 3.243 and 3.287 Å. The conductivity of Pd-SWCNTs before and after adsorption may change little because of the large interaction distance.

2.3.3. The analysis of the density of states and Frontier molecular orbital

Large charge transfer affects the density of states (DOS) near the Fermi level and brings about significant differences in frontier molecular orbitals [20]. To further elucidate the electronic properties of the Pd-SWCNTs and molecule-Pd-SWCNTs, total electronic density of states (TDOS) and local DOS of a group (Pd or molecule) (LDOS) are depicted to investigate the influence of gas adsorption [25] in **Figure 21**. To further study the electronic structure of the Pd-SWCNTs and molecule-Pd-SWCNTs near the Fermi level, the highest occupied molecular orbital (HOMO) and the lowest unoccupied molecular orbital (LUMO) in the molecule adsorption on the Pd-doped SWCNTs are listed in **Table 3**. The diagrams of HOMO and LUMO are depicted in **Figure 22**.

From **Figure 21**, we found that the LDOS of Pd atom has little contribution to each TDOS and that the changes of TDOS are mainly from the adsorbed molecules. As plotted in **Figure 21a1**, the DOS of Pd-doped SWCNTs is continuous at Fermi level, which suggests that Pd-doped SWCNTs is a conductor. Upon adsorption of SO_2 molecule in **Figure 21b1** and **b2**, the TDOS near Fermi level evidently increased, and the DOS at Fermi level was enhanced when the adsorbed SO_2 molecule increased. In **Figure 22b1**, the HOMO of the SO_2-Pd-SWCNTs was mainly constituted by the Pd and SO_2, and the p orbital of S and O atoms interacted with the d orbitals of the Pt atom. The LUMO is localized on the SWCNTs, as seen in **Figure 22b2**. After the other SO_2 molecule approached the Pd atom in **Figure 22b3** and **b4**, the LUMO significantly transferred to the SO_2 molecules. The HOMO-LUMO energy gap of the SO_2-Pd-SWCNTs is only 0.066 eV, which is 0.279 eV smaller than that of bare Pd-SWCNTs. Although the HOMO-LUMO energy gap of the $2SO_2$-Pd-SWCNTs is slightly bigger than single molecule adsorption, it was still 0.229 eV smaller than individual Pd-SWCNTs. The decrease of HOMO-LUMO energy gap associated with the significantly enhanced in the TDOS near the Fermi level

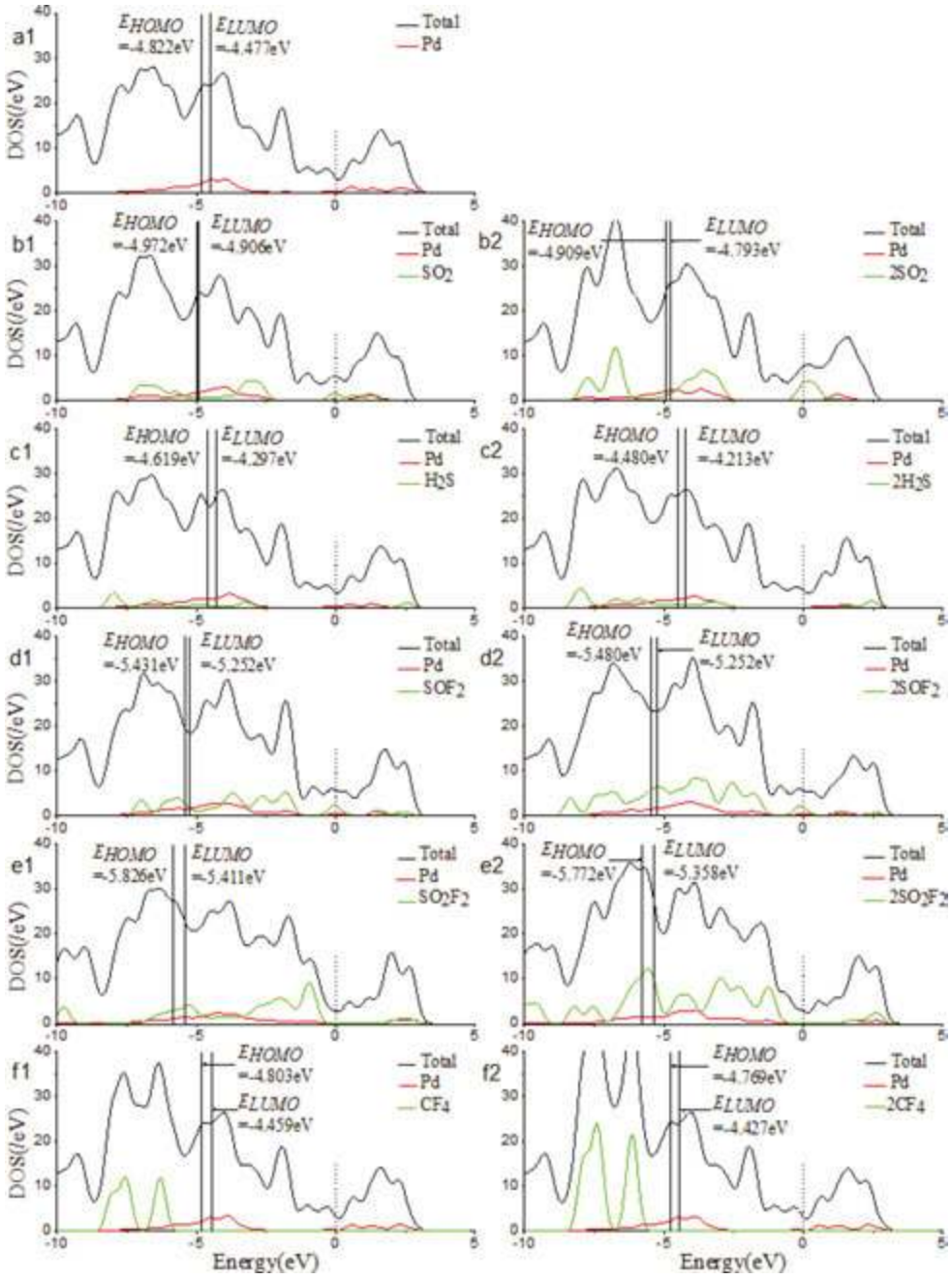

Figure 21. Total electronic density of states and local density of states for the Pd-SWCNTs and molecule-Pd-SWCNTs. Dash and solid lines indicate the Fermi level and HOMO-LUMO, respectively.

System	EHOMO (eV)	ELUMO (eV)	EL-H (eV)
Pd-SWCNTs	−4.822	−4.477	0.345
SO_2-Pd-SWCNTs	−4.972	−4.906	0.066
$2SO_2$-Pd-SWCNTs	−4.909	−4.793	0.116
H_2S-Pd-SWCNTs	−4.619	−4.297	0.322
$2H_2S$-Pd-SWCNTs	−4.480	−4.213	0.267
SOF_2-Pd-SWCNTs	−5.431	−5.252	0.179
$2SOF_2$-Pd-SWCNTs	−5.480	−5.252	0.228
$SO2F_2$-Pd-SWCNTs	−5.826	−5.411	0.415
$2SO2F_2$-Pd-SWCNTs	−5.772	−5.358	0.414
CF_4-Pd-SWCNTs	−4.803	−4.459	0.344
$2CF_4$-Pd-SWCNTs	−4.769	−4.427	0.342

Table 3. The HOMO, LUMO energy and HOMO-LUMO energy gap.

suggests that the adsorption of SO_2 largely increases conductance. According to the results reported by Camilli G et al. [26], using armchair Pd SWCNTs resulted in the reduction in the HOMO-LUMO energy gap of single and dual H_2S molecule adsorption by 0.17 and 0.16 eV, respectively. Meanwhile, the TDOS change introduced by the second SO_2 molecule showed no significant difference. Pd-doped zigzag SWCNTs show preferable sensitivity to SO_2.

According to the H_2S molecules adsorbed on Pd-SWCNTs, the TDOS at Fermi level showed no change whether single or dual H_2S adsorption in **Figure 21c1** and **c2** occurred. In **Figure 22**c1–c4, almost the entire HOMO and LUMO were on Pd-SWCNTs. The HOMO-LUMO energy gap of H_2S-Pd-SWCNTs and $2H_2S$-Pd-SWCNTs is 0.322 and 0.267 eV, respectively, which is slightly decreased compared with the bare Pd-SWCNTs. The results are consistent with the adsorption configurations. Given that the H atoms have formed a covalent bond with the S atom, the H_2S molecules can only interact with Pd-SWCNTs by S atoms. Although S atom forms the interaction with Pd atom, the primary S-H bond makes it hard to build strong interaction with the Pd-SWCNTs. The same result is seen in Pt-doped SWCNTs [27]. The small change at Fermi level in the H_2S adsorption process indicates little change in conductivity, which limits the performance of Pd-SWCNTs to detect the H_2S gas in SF_6 decomposition components.

Upon SOF_2 adsorption, as seen in **Figure 22d1** and **d2**, the p orbital of S atom and d orbital of Pt atom form a δ bonding orbital in the HOMO. In the LUMO, the p orbital of S atom in SOF_2 overlaps with the d orbital of Pt atom. The HOMO and LUMO energies of SOF_2-Pd-SWCNTs are slightly reduced with respect to those of bare Pd-SWCNTs. The HOMO-LUMO energy gap diminished to 0.179 eV. The decrease of the HOMO-LUMO energy gap would result in increased electron transfer to gas molecule. As we have already mentioned, the second SOF_2 molecule is far from the Pd atom. Therefore, the LDOS of the second SOF_2 brings little

http://dx.doi.org/10.5772/intechopen.68325

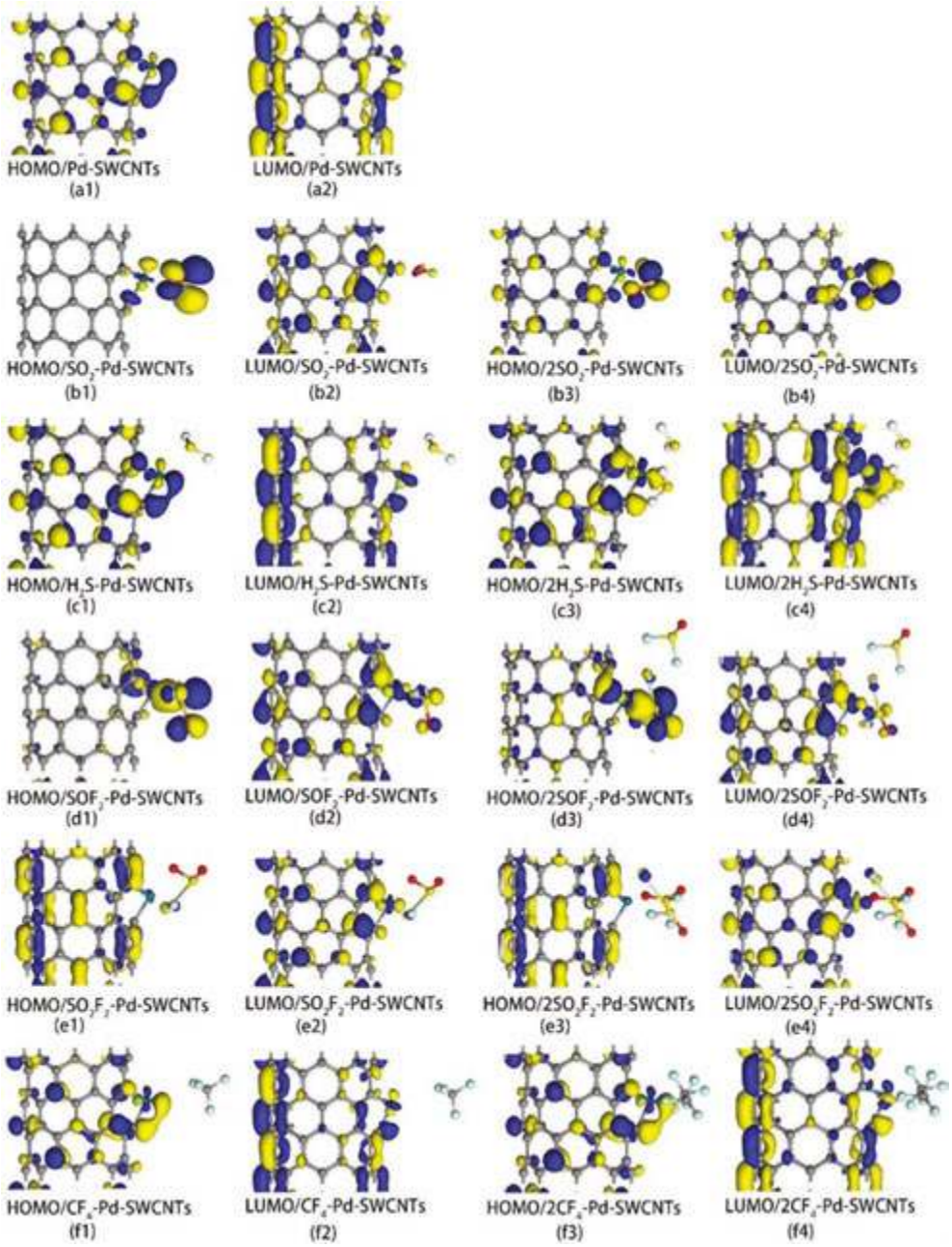

Figure 22. The HOMO and LUMO orbitals on Pd-SWCNTs and molecule-Pd-SWCNTs.

contribution to TDOS of adsorption system (**Figure 21d1** and **d2**). The HOMO and LUMO of 2SOF_2-Pd-SWCNTs in **Figure 22d3** and d4 have also confirmed the analysis results, neither the HOMO nor the LUMO is located on the second SOF_2 molecule. Therefore, conductivity does not increase with the rise of SOF_2 molecule number adsorbed on Pd-SWCNTs.

From the orbital of single SO_2F_2 adsorbed on Pd-SWCNTs in **Figure 22e1**, we can see a weak bond between the molecule and the Pd-SWCNTs. The HOMO-LUMO energy gap is 0.415 eV, which increased with the energy gap in other molecule adsorption. It greatly reduces the electron transition probability between HOMO and LUMO. Similar to the second SOF_2 adsorption, the adsorption system keeps its original characteristics after the second SO_2F_2 adsorbed on Pd-SWCNTs in **Figure 22e2**. In addition, the TDOS of SO_2F_2 adsorbed Pd-SWCNTs at the Fermi level is weaker than individual Pd-SWCNTs. Considering the molecule frontier orbital and TDOS, we assumed that SO_2F_2 adsorption will result in the decrease of conductance.

Upon the adsorption of CF_4, the LDOS introduced by CF_4 mainly under the Fermi level was not significant (**Figure 21f1** and **f2**). Furthermore, the HOMO and LOMO were almost identical to that of Pd-SWCNTs, as shown in **Figure 22f1–f4**. Considering the frontier orbital and TDOS, we predicted that the Pd-SWCNTs are insensitive to CF_4 detection.

2.3.4. Summary: gas adsorption on Pd-SWCNTs

Adsorption of SF_6 decomposed gas molecules (SO_2, H_2S, SOF_2, SO_2F_2 and CF_4) on Pd-doped (8, 0) SWCNTs was explored through density functional theory-based method. The geometrical and electronic structures, density of state and frontier molecular orbital were analyzed to predict the adsorption properties and mechanism of complexes.

In the adsorption of SO_2, strong binding energy between SO_2 and Pd-SWCNTs indicates the nature of chemical adsorption. The adsorption energy increases with the rise of SO_2 molecule number adsorbed on Pd-SWCNTs. The large contribution of SO_2 and the total DOS near the Fermi level is responsible for the conductance increase of SO_2-Pd-SWCNTs. The high adsorption sensitivity of Pd-SWCNTs makes it suitable for SO_2 detection.

For the adsorption SOF_2, F-end adsorption conformation is energetically favorable. The large formation energy and structure change show that the SOF_2 molecule is chemically bonded to Pd-doped SWCNTs. The large enhancement toward the Fermi level induced by the LDOS of SOF_2 implies the increase of conductance for the SO_2-Pd-SWCNTs. However, the strong repulsive force between the SOF_2 molecules limits it is further adsorption, and therefore, the increased conductivity introduced by SOF_2 is smaller than SO_2.

Upon the adsorption of one SO_2F_2 to the Pd-SWCNTs, the HOMO-LUMO energy gap of the SO_2F_2-Pd-SWCNTs increased to 0.415 eV, which is larger than that of the Pd-SWCNTs, whereas the TDOS at Fermi level slightly decreased. The command action of the HOMO-LUMO energy gap and TDOS finally led to the conductivity decrease of the SO_2F_2 adsorbed Pd-SWCNTs.

When CF_4 is adsorbed on Pd-SWCNTs, the HOMO-LUMO energy and TDOS remained unchanged based on our computation. The Pd-CNT showed low sensitivity for CF_4 gas.

Results of the theoretical calculation showed that Pd-SWCNTs had different sensitivity to the SF_6 decomposition gases. After SO_2, H_2S and SOF_2 were adsorbed on Pd-SWCNTs, the conductivity increases in the following order: $SO_2 > SOF_2 > H_2S$. The conductivity of SO_2F_2 decreased when it was adsorbed by Pd-SWCNTs. Conversely, Pd-SWCNTs are not sensitive to the other gas molecule CF_4. Through changes in conductivity, the Pd-SWCNTs achieved selective detection of five SF_6 decomposition gases: SO_2, H_2S, SOF_2, SO_2F_2 and CF_4.

2.4. Gas-sensing properties of Ni-SWCNTs to SOF_2, SO_2F_2, SO_2, H_2S, HF, CF_4 and SF_6

2.4.1. Structural parameters of intrinsic Ni-SWCNTs

After an individual Ni atom was decorated onto the SWCNTs and relaxed to stable structure, the Ni atom distinctly protruded out of the SWCNTs sidewall due to the large Ni atom radius compared with that of SWCNTs as shown in **Figure 23** [28]. The bond length C3-Ni was stretched to 1.84 Å, and the bond length C4-Ni length along the axial of Ni-SWCNTs increased to 1.76 Å.

2.4.2. The analysis of gas adsorption structure

After the optimization of individual Ni-SWCNT and gas molecules, the gas molecules were relaxed to various sites on the surface of Ni-SWCNTs to get the lowest energy structure [11]. Moreover, in order to fully analyze the influence brought by decomposed products, adsorption of both single and double gas molecules was studied in this work [11]. As seen in **Figure 24**, it was found that all of the gas molecules intended to be adsorbed at the Ni-doped site, which acted as an active site for adsorption [11]. To analyze the adsorption properties, the banding distance D, binding energy E_{ads} and charge transfer Q_t were obtained as shown in **Table 4** [11]. D presented the nearest distance between the adsorbed gas molecules and the surface of Ni-SWCNTs, where D_1 and D_2, respectively, represented the distances for two different

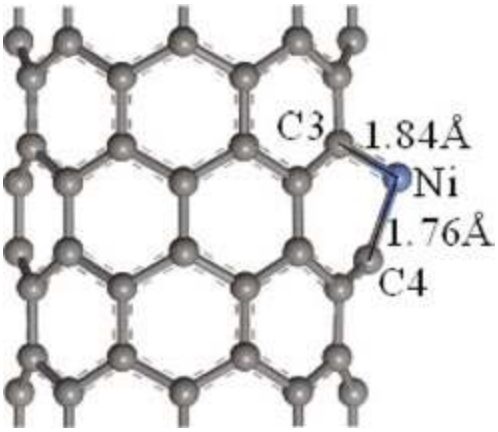

Figure 23. Geometric structures of Ni-doped SWCNTs after optimization. The structural parameters are shown as Å.

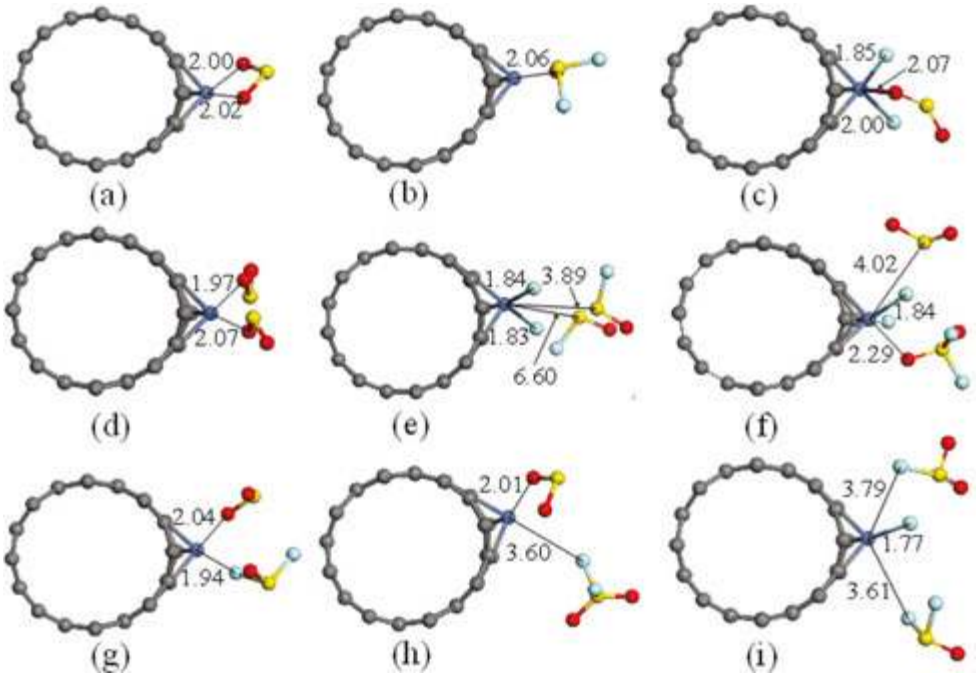

Figure 24. Most stable geometries of gas molecules interacting with Ni-doped SWCNTs (distances in Å).

molecules. Similarly, the charge transferred from gas molecules to Ni-SWCNTs was labeled as Q_t, Q_{t1} and Q_{t2} referred to the charge transfer for these two different molecules. All the negative value of E_{ads} implied that the adsorption was exothermic and occurred spontaneously.

System	D_1 (Å)	D_2 (Å)	Q_{t1} (e)	Q_{t2} (e)	E_{ads} (eV)
SWCNTs/SO_2	2.00	\	−0.35	\	−1.13
SWCNTs/SOF_2	2.06	\	−0.06	\	−0.49
SWCNTs/SO_2F_2	2.07	\	−0.94	\	−1.93
SWCNTs/2SO_2	1.97	2.07	−0.24	−0.08	−1.50
SWCNTs/2SOF_2	3.89	6.60	−0.51	−0.50	−1.79
SWCNTs/2SO_2F_2	2.29	4.02	0.06	−0.83	−2.16
SWCNTs/ SO_2&SOF_2	1.94	2.04	−0.31	−0.09	−0.71
SWCNTs/ SO_2&SO_2F_2	2.01	3.60	−0.35	0	−1.14
SWCNTs/ SOF_2&SO_2F_2	3.61	3.79	0	−0.71	−0.45

Table 4. Adsorption energy E_{ads}, charge transfer Q_t from adsorbed gas molecules to Ni-SWCNTs.

As shown in **Table 4** and **Figure 24a–c,** single SO_2, SOF_2 and SO_2F_2 molecules were adsorbed onto SWCNTs. The oxygen atoms of both SO_2 and SOF_2 were close to the Ni atom with the nearest bond length of 2.00 and 2.06 Å because of the strong electronegativity of oxygen atom [11]. And the sulfur atom was further away from the Ni-SWCNTs sidewall because it built a stable covalent bond with oxygen atoms and fluorine atoms, making it hard to interact with the Ni atom [11]. The structures of SO_2 and SOF_2 were almost kept unchanged in the adsorption process. The low E_{ads} values of SO_2 and SOF_2 indicate that the adsorption of SO_2 and SOF_2 is physisorption, which can also be verified by the long reaction length. However, when one SO_2F_2 molecule was close to Ni-SWCNTs, the S—F bond was broken, resulting in building a new Ni—F bond [11]. The binding distance from the newly formed SO_2 to the surface of the Ni-SWCNTs was 2.07 Å [11]. The E_{ads} reached −1.93 eV, which nearly tripled the E_{ads} value of SOF_2, and doubled that of SO_2. Based on the obvious structure deformation and large E_{ads}, we conclude that the interaction between SO_2F_2 and Ni-SWCNTs is chemisorption.

As to the adsorption of two identical gas molecules, as seen in **Table 4** and **Figure 24d–f**, the double SO_2 adsorption was similar to that of single SO_2 molecule with a nearest bond length of 1.97 Å [11]. Interestingly, the structures of both SOF_2 molecules were deformed with two new SOF molecules produced in the adsorption process, indicating that the Ni-doped metal showed great adsorption ability [11]. According to the SO_2F_2 adsorption, one of the SO_2F_2 molecules deformed to one SO_2 and two fluorine atoms that were adsorbed on Ni atom [11]. And the other SO_2F_2 molecule was close to the Ni atom with a binding distance of 2.29 Å [11]. The E_{ads} of double SO_2, SOF_2 and SO_2F_2 was −1.50, −1.79 and −2.16 eV, respectively, which were increased compared with that of corresponding single molecule adsorption. In general, two SO_2 molecules are physically adsorbed onto Ni-SWCNTs, and the interactions for SOF_2 and SO_2F_2 are chemisorption deducing form the obviously structure changes.

As for the adsorption of two foreign gas molecules on Ni-SWCNTs shown in **Table 4** and **Figure 24g–i**, there was no significant difference in the adsorption length for SO_2 compared with that of single and double SO_2 adsorption in **Figure 24a** and d. It should be noticed that the molecule structures of SOF_2 (**Figure 24g**) and SO_2F_2 (**Figure 24h**) kept unbroken, while in the SOF_2 and SO_2F_2 case in **Figure 24i**, one fluorine broke up from SO_2F_2 and was adsorbed on the Ni atom, and the SOF_2 molecule was away from the sidewall of Ni-SWCNTs with an adsorption length of 3.61 Å.

2.4.3. The analysis of the density of states and frontier molecular orbital

2.4.3.1. Adsorption of single decomposed gas molecule on the surface of Ni-SWCNT

According to the detection mechanism of chemiresistor sensor, the conductivity of gas-sensing materials changes in response to the different gas molecules [11]. Using the density of states (DOS) and frontier molecular orbital theory, the factors influencing the change of conductivity can be found directly [11]. We first analyze the single gas molecule adsorption cases, including SO_2, SOF_2 and SO_2F_2 (**Figure 24a–c**). Along with the charge transfer between the gas molecules and Ni-SWCNTs, the total density of states (TDOS), the highest occupied molecular orbital (HOMO) and the lowest unoccupied molecular orbital (LUMO) were distinctly changed [11]. If the energy gap between HOMO and LUMO narrows down, the charge

carrier transfer becomes easier from HOMO to LUMO. Then, the conductivity of adsorption system increases correspondingly [11].

The continuous TDOS of Ni-SWCNTs shown in **Figure 25a** is consistent with the verified results that intrinsic Ni-SWCNTs possess good conductivity after Ni atom doping. Bak et al. reported that mesoporous nickel/CNTse hybrid material showed high conductivity [29]. Comparing TDOS before (**Figure 25a**) and after (**Figure 25b**) the SO_2 molecule adsorption on the surface of Ni-SWCNTs, there is no significant change of TDOS at the energy levels that are far below or far above the Fermi level, and the main change is located at the energy level that is slightly above the Fermi level, which is attributed to the SO_2 adsorption that increases the number of effective charge. For the case with SOF_2 molecule adsorption, the TDOS almost does not change below the Fermi level as shown in **Figure 25c**. Although the TDOS far above the Fermi level slightly increases, it has no contribution to the change of conductivity, which agrees with the low interaction energy discussed above. For the adsorption of single SO_2F_2 (**Figure 25d**), the TDOS increases below the Fermi level and decreases above the Fermi level due to the chemisorption.

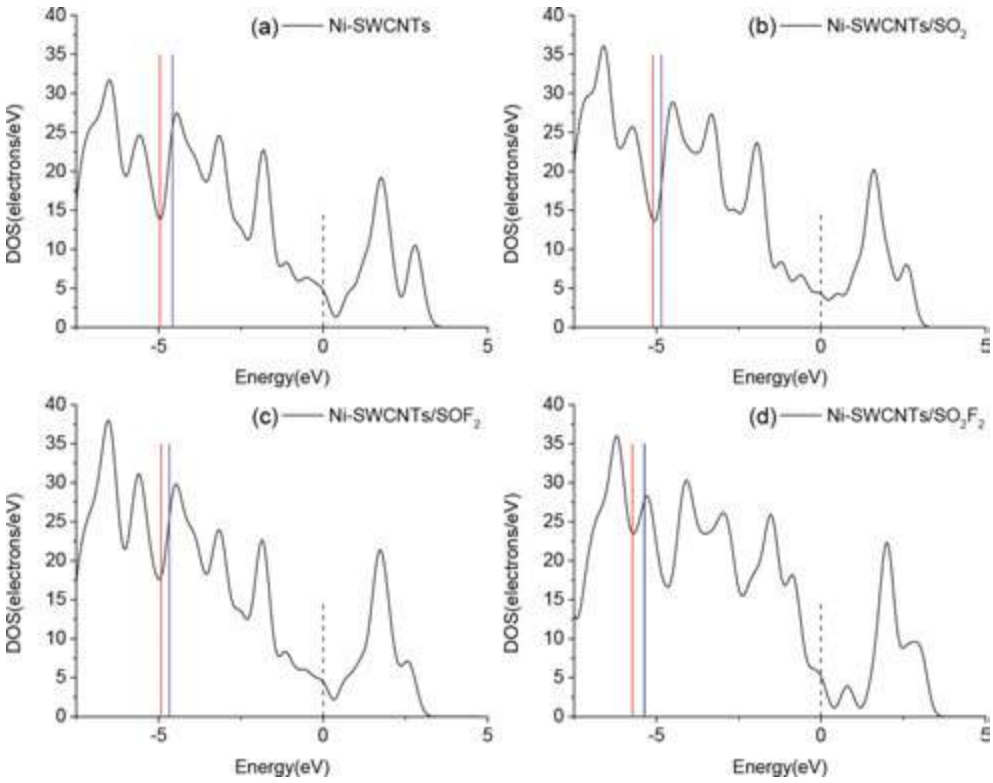

Figure 25. Comparison of the TDOS for (a) intrinsic Ni-SWCNTs, (b) SO_2 adsorbed Ni-SWCNTs, (c) SOF_2 adsorbed Ni-SWCNTs and (d) SOF_2 adsorbed Ni-SWCNTs. The left solid line is HOMO while the right solid line is LUMO, and the dash line is Fermi level.

The HOMO, LUMO, E_g for intrinsic Ni-SWCNTs and the materials with single gas molecule adsorption are reported in **Table 5** [11]. It is found that E_g was reduced at different extent for all gas adsorption process, making the charge easier to transfer for the adsorption system. Before each gas molecule approached to the surface of Ni-SWCNTs, the HOMO and LUMO were mainly distributed on the Ni-doped side and its opposite side (**Figure 26a1** and **a2)** with 0.38 eV E_g. For the physisorption of SO_2, the HOMO and LUMO were slightly transferred to the SO_2 adsorption site as shown in **Figure 26b1** and **b2** and became more uniformly distributed on the surface of Ni-SWCNTs. In addition, the E_g was narrowed down to 0.26 eV. Agreeing with the increase of TDOS, we conclude that the conductivity would increase with the single SO_2 adsorption. The increase result is agree with the conclusion reported by Yu et al. that SO_2 molecules adsorption on the surface of SWCNTs increases the conductivity [30]. When single SOF_2 molecule adsorbed on Ni-SWCNTs, the E_g was reduced to 0.25 eV, which was comparable to the SO_2 adsorption case. Comparing HOMO and LUMO of SOF_2 adsorption system (presented in **Figure 26c1** and **c2**) with that of intrinsic NI-SWCNTs, the HOMO and LUMO were nearly not changed except the slight change of LUMO due to SOF_2 molecule. Considering the weak adsorption energy, unchanged TDOS and frontier molecular orbital comprehensively, single SOF_2 adsorption has no influence on the conductivity of Ni-SWCNTs system. For SO_2F_2 adsorption, the E_g value (0.37 eV) was almost the same as that

System	LUMO	HOMO	E_g (eV)
SWCNTs	−4.58	−4.96	0.38
SWCNTs/SO_2	−4.85	−5.11	0.26
SWCNTs/SOF_2	−4.67	−4.92	0.25
SWCNTs/SO_2F_2	−5.36	−5.73	0.37

Table 5. HOMO, LUMO, E_g of intrinsic Ni-SWCNTs and single gas molecule adsorption.

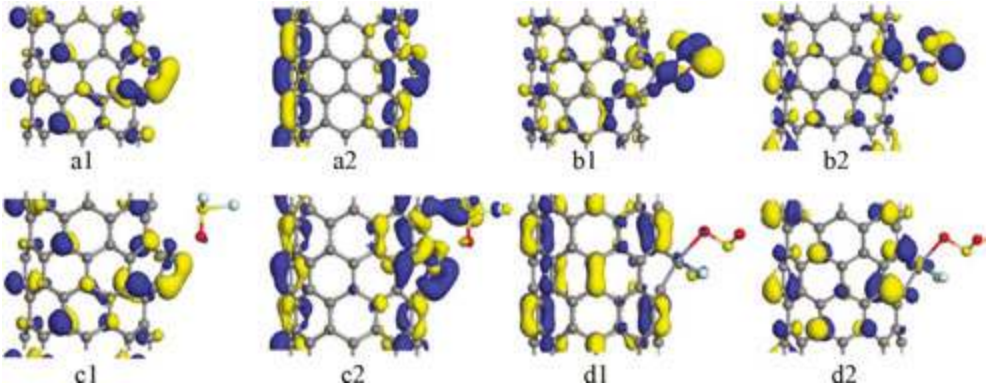

Figure 26. The HOMO and LUMO: (a1) and (a2) intrinsic Ni-SWCNTs; (b1) and (b2) SO_2 adsorbed Ni-SWCNTs; (c1) and (c2) SOF_2 adsorbed Ni-SWCNTs; (d1) and (d2) SO_2F_2 adsorbed Ni-SWCNTs.

of pure Ni-SWCNTs, and the HOMO and LUMO were distinctly reduced as listed in **Table 5**. The configurations of HOMO and LUMO of SO_2F_2 adsorbed Ni-SWCNTs with chemisorption are summarized in **Figure 26d1** and **d2**, and there are few orbital surrounding the adsorbed SO_2F_2. The strong chemical bond between Ni atom and SO_2F_2 impedes the free transportation of charge and reduces the free charge of Ni atom at the same time. In other words, the chemisorption of SO_2F_2 reduces the conductivity, which is consistent with the results of TDOS analysis. The decrease result is also confirmed by our previous research that SO_2 adsorption reduces the conductivity of Pd-doped SWCNTs [31].

2.4.3.2. Adsorption of double identical decomposed gas molecule on the surface of Ni-SWCNT

In practical situation, the insulated SF_6 gas may simultaneously decompose to SO_2, SOF_2 and SO_2F_2, indicating that it is mixed gas in SF_6 insulated equipment. Therefore, the multiple gas molecule adsorption was considered in our study. With the limited adsorption ability of single Ni-doped SWCNTs, double gas molecule adsorption is sufficient to analyze the situation of multiple gas molecule adsorption. The influence on conductivity brought by absorption of double identical decomposed gas molecules is discussed first. Comparison of the TDOS before and after gas molecule adsorption is shown in **Figure 27**. The presence of Ni active site leads to double identical SO_2 simultaneously adsorbed on Ni-SWCNTs, resulting in an enhancement of the communization movement between the Ni-SWCNTs and adsorbed gas molecules. As can be seen form **Figure 27a** and **b**, the TDOS was improved in all energy distribution zone, although the TDOS just above the Fermi level changed little, but that below the Fermi level increased, which means that the major carrier transfer from the valence band and the conduction band is enhanced. When the double identical SOF_2 and SO_2F_2 molecules interacted with Ni-SWCNTs by chemisorption, the TDOS near the Fermi level reduced. It can be seen in **Figure 27c**, the decrease area of TDOS for SOF_2 adsorption is slightly below the Fermi level, while a sharp TDOS reduction occurs above the Fermi level for SO_2F_2 adsorption as shown in **Figure 27d**.

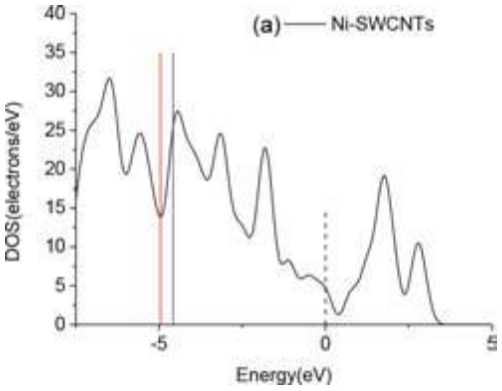

Figure 27. Comparison of the TDOS for double identical molecules: (a) intrinsic Ni-SWCNTs, (b) double SO_2 adsorbed Ni-SWCNTs, (c) double SOF_2 adsorbed Ni-SWCNTs and (d) double SOF_2 adsorbed Ni-SWCNTs. The left solid line is HOMO while the right solid line is LUMO, and the dash line is Fermi level.

Table 6 presents the results of the LUMO and HOMO energies of the double identical SF_6 decomposed products (SO_2, SOF_2 and SO_2F_2) adsorption on the surface of Ni-SWCNTs based on DFT calculation. All of the energy of HOMO and LUMO declined during the adsorption process. Considering the distribution of frontier molecular orbital for double SO_2 physisorption in **Figure 28b1** and **6b2**, the HOMO evenly distributed on the structure of Ni-SWCNTs. In addition, the E_g was declined from 0.38 eV (intrinsic SWCNTs) to 0.26 eV (SWCNTs/2SO_2). The computed TDOS and frontier molecular orbital reveal that the physisorption between double SO_2 and Ni-SWCNTs enhances the conductivity, which is consistent with the result of single SO_2 adsorption. The distribution of HOMO and LUMO for double SOF_2 adsorption signally changed as displayed in **Figure 28c1** and **6c2**. The HOMO has completely transferred to two newly produced SOF molecules. Conversely, the LUMO entirely locates on the surface of Ni-SWCNTs. As we have discussed above, two SOF molecules were far away from the surface of Ni-SWCNTs. So it was hard for charge carrier to transfer between HOMO and LUMO, though the E_g was greatly reduced to 0.08 eV. Comparing with the unchanged conductivity of the single SOF_2 adsorption case, the adsorption of double SOF_2 molecules slightly reduced the conductivity. From **Figure 28d1** and **6d2**, we found neither the HOMO nor the LUMO located around gas adsorption site, because the strong chemical bond interaction prevents the charge carrier from transferring freely. The HOMO evenly distributed on carbon atoms,

System	LUMO	HOMO	E_g (eV)
SWCNTs	−4.58	−4.96	0.38
SWCNTs/2SO_2	−5.03	−5.29	0.26
SWCNTs/2SOF_2	−5.52	−5.60	0.08
SWCNTs/2SO_2F_2	−5.02	−5.48	0.46

Table 6. HOMO, LUMO, E_g of intrinsic Ni-SWCNTs and double identical gas molecules adsorption.

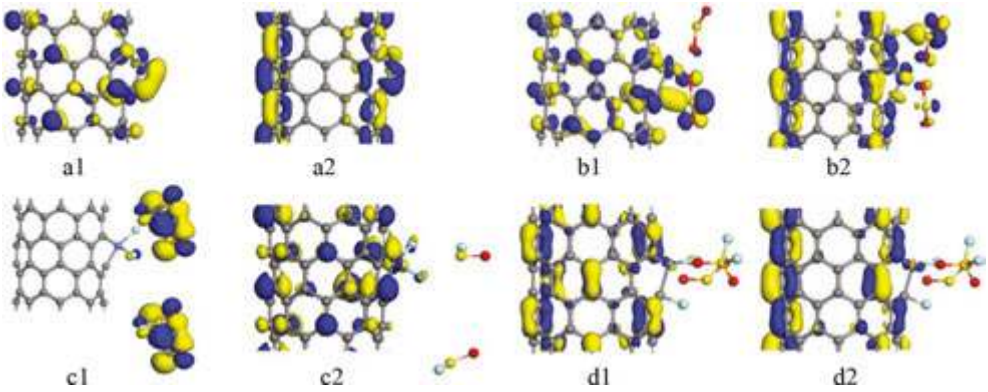

Figure 28. The HOMO and LUMO: (a1) and (a2) intrinsic Ni-SWCNTs; (b1) and (b2) double SO_2 adsorption; (c1) and (c2) double SOF_2 adsorption; (d1) and (d2) double SO_2F_2 adsorption.

and it increased compared with that of intrinsic Ni-SWCNTs. While the distribution of LUMO on carbon atoms kept unaltered. Along with the change of the HOMO and LUMO, the E_g was increased to 0.46 eV. We conclude that the double identical SO_2F_2 adsorption reduces the conductivity of Ni-SWCNTs.

2.4.3.3. Adsorption of double foreign decomposed gas molecule on the surface of Ni-SWCNT

In case of mixed gas decomposed in SF_6 insulated equipment, the mixed gas molecules could also be adsorbed on the surface of Ni-SWCNTs with double foreign gas molecules except the double identical adsorption case discussed above. According to the TDOS shown in **Figure 29**, the change of TDOS presents significant difference comparing with that of single and double identical gas molecules adsorption. All of the TDOS near the Fermi level has increased. As discussed in the geometry analysis for SO_2&SOF_2 adsorption, both gas molecules move close to the surface of Ni-SWCNTs by physisorption. The sharply increased TDOS above the Fermi level (see **Figure 29b**), which is even bigger than that of single SO_2 adsorption implies the prominent improvement of conductivity. And the change of conductivity is agreed with the literature that reported the increase of conductivity during SO_2 gas detection [30]. When SO_2&SOF_2 interacted with Ni-SWCNTs, the SOF_2 molecule was away from the surface of Ni-SWCNTs according to the structure discussed before. Comparing the TDOS of SO_2&SO_2F_2 adsorption (**Figure 29c**) with that of single SO_2, we found that the change of TDOS presents identical increase trend, deriving from the crucial role of SO_2 adsorption. For the adsorption of SOF_2&SO_2F_2, only the broken fluorine atom and one SOF_2 made contribution to the change of conductivity. As the TDOS of SOF_2&SO_2F_2 adsorption depicted in **Figure 29d**, the TDOS near the Fermi level and site of the HOMO and LUMO increased.

All of the increased TDOS for mixed gas molecule adsorption is consistent with the frontier molecular orbital analysis in **Figure 30**. It can be seen obviously that the HOMO and LUMO distribution (see **Figure 30b** and **Table 7**) has extended to the surface of adsorbed SO_2 and SOF_2

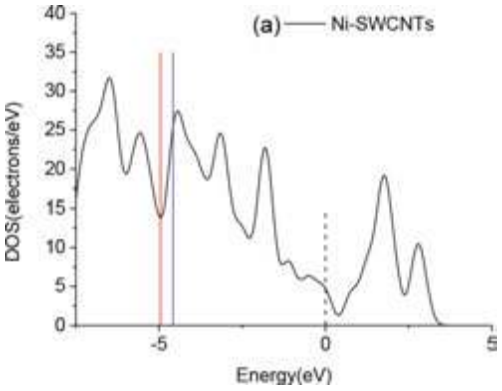

Figure 29. Comparison of the TDOS for double foreign molecules: (a) intrinsic Ni-SWCNTs; (b) SO_2, SOF_2 adsorbed Ni-SWCNTs; (c) SO_2, SO_2F_2 adsorbed Ni-SWCNTs and (d) SOF_2, SO_2F_2 adsorbed Ni-SWCNTs. The left solid line is HOMO while the right solid line is LUMO, and the dash line is Fermi level.

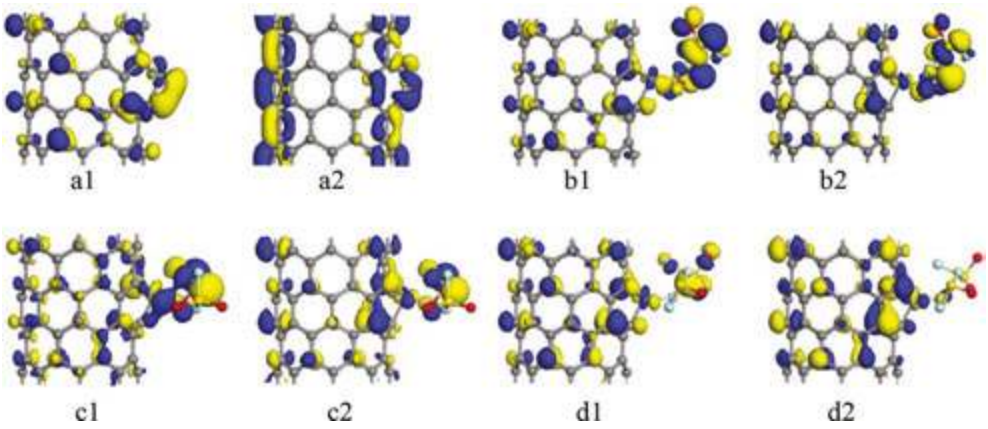

Figure 30. The HOMO and LUMO: (a1) and (a2) intrinsic Ni-SWCNTs; (b1) and (b2) SO_2, SOF_2 adsorption; (c1) and (c2) SO_2, SO_2F_2 adsorption; (d1) and (d2) SOF_2, SO_2F_2 adsorption.

molecules, and the E_g has narrowed to 0.20 eV. So the charge carrier transportation increases correspondingly, which also confirms the enhanced TDOS. Thus, we conclude that the effect of SO_2 and SOF_2 adsorption significantly improves the conductivity of Ni-SWCNTs. Although the SO_2F_2 molecule was too far to affect the frontier molecular orbital (see **Figure 30c**), the adsorbed SO_2 was efficient to enhance the conductivity by reducing the energy barrier E_g (0.26 eV) and increasing the HOMO and LUMO distribution. For the HOMO and LUMO distribution of SOF_2&SO_2F_2 adsorption shown in **Figure 19d**, part of HOMO distributed on the surface of bonded fluorine and one SOF_2 molecule. And the LUMO distribution became uniform on carbon atoms comparing with that of intrinsic Ni-SWCNTs. Besides, the TDOS at site of HOMO and HOMO increased as seen in **Figure 29d** with E_g dropped to 0.21 eV. Taking account of the changed distribution of TDOS and frontier molecular orbital that benefits charge carrier transportation, the adsorption of SOF_2&SO_2F_2 increases the conductivity.

2.4.4. Summary: gas adsorption on Ni-SWCNTs

In summary, the adsorption effects of typical decomposition products: SO_2, SOF_2 and SO_2F_2 in SF_6 insulated equipment toward Ni-doped (8, 0) zigzag SWCNTs have been theoretically investigated using first-principle calculation based on PBE function of DFT. It is found that

System	LUMO	HOMO	E_g (eV)
SWCNTs	−4.58	−4.96	0.38
SWCNTs/SO_2&SOF_2	−4.82	−5.02	0.20
SWCNTs/SO_2&SO_2F_2	−4.85	−5.11	0.26
SWCNTs/SOF_2&SO_2F_2	−5.28	−5.49	0.21

Table 7. HOMO, LUMO, E_g of intrinsic Ni-SWCNTs and double foreign gas molecules adsorption.

the gas molecules tend to approach the surface of Ni-SWCNTs at the Ni-doped active site with the improved adsorption ability to gas molecules. The density of state and frontier molecular orbital were adopted to study the physical properties of Ni-SWCNTs before and after gas molecules adsorption. Comparing the change of conductivity in different adsorption situations, the conductivity of Ni-SWCNTs increases in the following order: SO_2 > SOF_2 after SO_2 and SOF_2 adsorbed onto Ni-SWCNTs. Conversely, SO_2F_2 adsorption onto Ni-SWCNTs slightly decreases conductivity. The following specific conclusion can be drawn.

For single decomposed gas molecule adsorption, SO_2 and SOF_2 interact with Ni-SWCNTs via physisorption, while SO_2F_2 strongly chemisorbed on Ni-SWCNTs. For SO2 adsorption, the TDOS near the Fermi level and the HOMO and LUMO increases with a declined E_g, resulting in the increase of conductivity. Conversely, the conductivity reduces after the SO_2F_2 absorption. And single SOF_2 made little contribution to the change of conductivity.

For the adsorption of double identical gas molecules, the double SO_2 is still physically adsorbed on Ni-SWCNTs, and the chemisorption acts on both SOF_2 and SO_2F_2. Considering the conductivity features, we conclude that the double SO_2 molecules increase the conductivity, while double SOF_2 and double SO_2F_2 adsorption show a decrease effect to conductivity.

The results of gas-sensing properties to mixed gas molecule adsorption have showed that the conductivity increases at different extent, reflecting the sensing specific to different gas molecules. In case of SO_2 and SOF_2 and SO_2 and SO_2F_2 adsorption, the improvement of conductivity is mainly derived from the contribution of SO_2 adsorption, which has also been founded in single and double SO_2 adsorption. For SOF_2 and SO_2F_2 adsorption, the Ni active site bonded with a fluorine broke form SO_2F_2 and the other two SOF_2 molecules away from the surface of Ni-SWCNTs, resulting in the increase of conductivity due to the evenly distributed LUMO.

Taking advantage of the sensing mechanism of Ni-SWCNTs to SF_6 decomposed products: SO_2, SOF_2 and SO_2F_2, the Ni-SWCNTs gas chemiresistor sensor can be prepared to realize the online detection and diagnosis of insulated faults in SF_6 insulated equipment.

2.5. Gas-sensing properties of Al-SWCNTs to SOF_2, SO_2F_2, SO_2, H_2S, HF, CF_4 and SF_6

2.5.1. Structural parameters of intrinsic Al-SWCNTs

When a carbon atom C1 was substituted by an Al atom, significant geometric changes occurred in Al-SWCNTs, as shown in **Figure 31**. Considering that the radius of the Al atom is larger than that of the carbon atom, the Al heteroatom protruded from the Al-SWCNT surface after structural optimization [32]. The bond length between Al─C3 and Al─C4 atoms reached 1.908 and 1.841 Å, respectively. The calculation results were similar to that of other research [17, 32, 33].

2.5.2. The analysis of gas adsorption structure

Following the optimization of each initial structure, all gas molecules were allowed to relax on the surface of Al-doped SWCNTs [32]. Cause the orientational effects play important role on the adsorption results. In addition, in order to receive the global minimum-energy structures

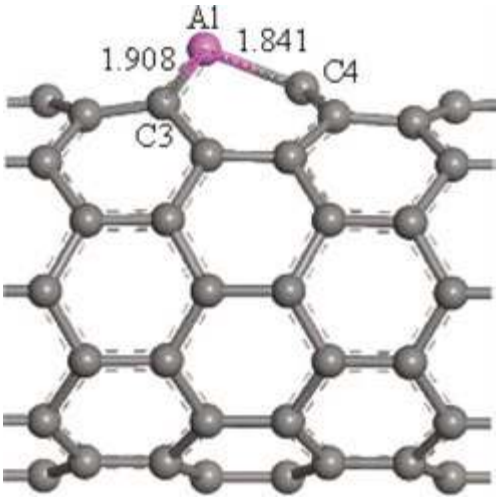

Figure 31. Geometric structures of Al-doped SWCNTs after optimization. The structural parameters are shown as Å.

from the all these minimum-energy structures, which may contain some local minimum-energy structures. Various adsorption sites and approaching ways of decomposition products were calculated to get the most minimum-energy structures, which are used as the most stable structure for each gas molecule adsorption in our study (**Figure 32**) [32]. The results showed that all of the gas molecules tended to adsorb at the site of Al atom, which revealed the stronger adsorption of Al atom than other undoped sites. Given that the electrical properties of SWCNTs could be significantly influenced by gas adsorption [32, 34], the strong adsorption provided an opportunity for the detection of SF_6 decomposition products based on the change of conductivity [32].

The adsorption energy E_{ads}, charge transfer Q_T and interactive distance d were computed to analyze the gas adsorption properties, which are shown in **Table 8**. We determined that all of the molecules have negative adsorption energy, indicating that the adsorption reaction was an exothermic process that occurred spontaneously [35]. In the adsorption process of the SOF_2 and SO_2F_2 gas molecules, the strong interaction decomposed SOF_2 and SO_2F_2 into other gas molecules. Thus, the binding distance from the SOF_2 and SO_2F_2 gas molecules to Al-SWCNTs is not shown in **Table 8**.

As shown in **Figure 32a1** and **a2** and **Table 8** [32], when one SO_2 molecule approached the surface of Al-SWCNTs in a different direction, two oxygen atoms were close to the Al atom. Meanwhile, the sulfur atom is far from the Al atom because the sulfur atom has already built a strong double bond with adjacent oxygen atoms. This steady interaction does not allow the sulfur atom to form another coordinate bond with the Al atom. The bond distance and angle of the SO_2 molecule slightly changed during the adsorption process, which corresponded with the result of a previous study [32, 36]. In the present study, the interaction distance between SO_2 molecule and Al atom was 1.988 Å, which is slightly smaller than that of Pd-doped (8, 0) SWCNTs [37] because the radius of the Al atom is smaller than that of the Pd atom [32]. Long gas

System	Structure	E_{ads} (eV)	Q_T (e)	d_1 (Å)	d_2 (Å)
SO_2	(a1)	−1.606	−0.493	1.988	–
$2SO_2$	(a2)	−2.206	−0.706	1.787	1.868
H_2S	(b1)	−1.051	0.234	2.47	–
$2H_2S$	(b2)	−1.498	0.273	2.425	3.495
SOF_2	(c1)	−2.103	−0.573	–	–
$2SOF_2$	(c2)	−2.974	−1.102	–	–
SO_2F_2	(d1)	−3.408	−1.041	–	–
$2SO_2F_2$	(d2)	−4.952	−3.018	–	–
CF_4	(e1)	−0.033	−0.003	3.27	–
$2CF_4$	(e2)	−0.087	0.019	2.710	3.537

Table 8. Calculated adsorption energy, charge transfer and binding distance from an Al atom to adsorbates.

interaction distance (1.988 Å) and low banding energy (−1.606 eV) indicated that the adsorption was some type of physisorption [32, 38]. When the second SO_2 molecule was adsorbed on Al-SWCNTs, the SO_2 molecules approached the Al atom with only one oxygen atom because of the repulsive interaction between the two gas molecules. The adsorption energy increased to 2.206 eV, with adsorption distances of 1.787 and 1.868 Å to the Al atom [32].

The adsorption structures and parameters of single and double H_2S molecules on Al-SWCNTs are shown in **Figure 32b1** and **b2** and **Table 8** [32]. After the relaxation process, a quasi-tetrahedron geometry around the Al center was observed. The hydrogen atoms and sulfur atom in the H_2S molecule generated strong bond energy [39]. Thus, the interaction between hydrogen atoms and Al was weak. Meanwhile, the sulfur atom could still react with the Al atom because of its multivalent feature. As such, the H_2S molecule approached the Al atom through the sulfur atom. The interaction distance between the S and Al atoms was approximately 2.47 Å, with the H─Al distance of 2.85 Å [32]. Considering the long interaction distance and low binding energy of −1.051 eV, the interaction indicated a moderate physisorption. When double H_2S molecules adsorbed on the surface of Al-SWCNTs, we observed that one molecule was distinctly far from the surface with a distance of 3.495 Å because of the repulsive force between molecules [32]. However, the adsorption site of the other H_2S molecule changed slightly compared with the former single molecule adsorption. The distance from the new added H_2S molecule to the doped Al atom was approximately 2.425 Å. The binding energy between single H_2S and Al-SWCNTs was approximately −1.051 eV, whereas the binding energy between double H_2S and Al-SWCNTs increased to −1.498 eV [32]. The Mulliken population analysis indicated that 0.234 and 0.273 electrons transferred from single and double H_2S molecules to Al-SWCNTs, respectively. In addition, our results were similar to the results of previously studied Au-doped SWCNTs [32, 40], in which the structural parameters, binding energy and charge transfer were also reported. Small difference between our results and than in previous report was found probably because different models were used in the

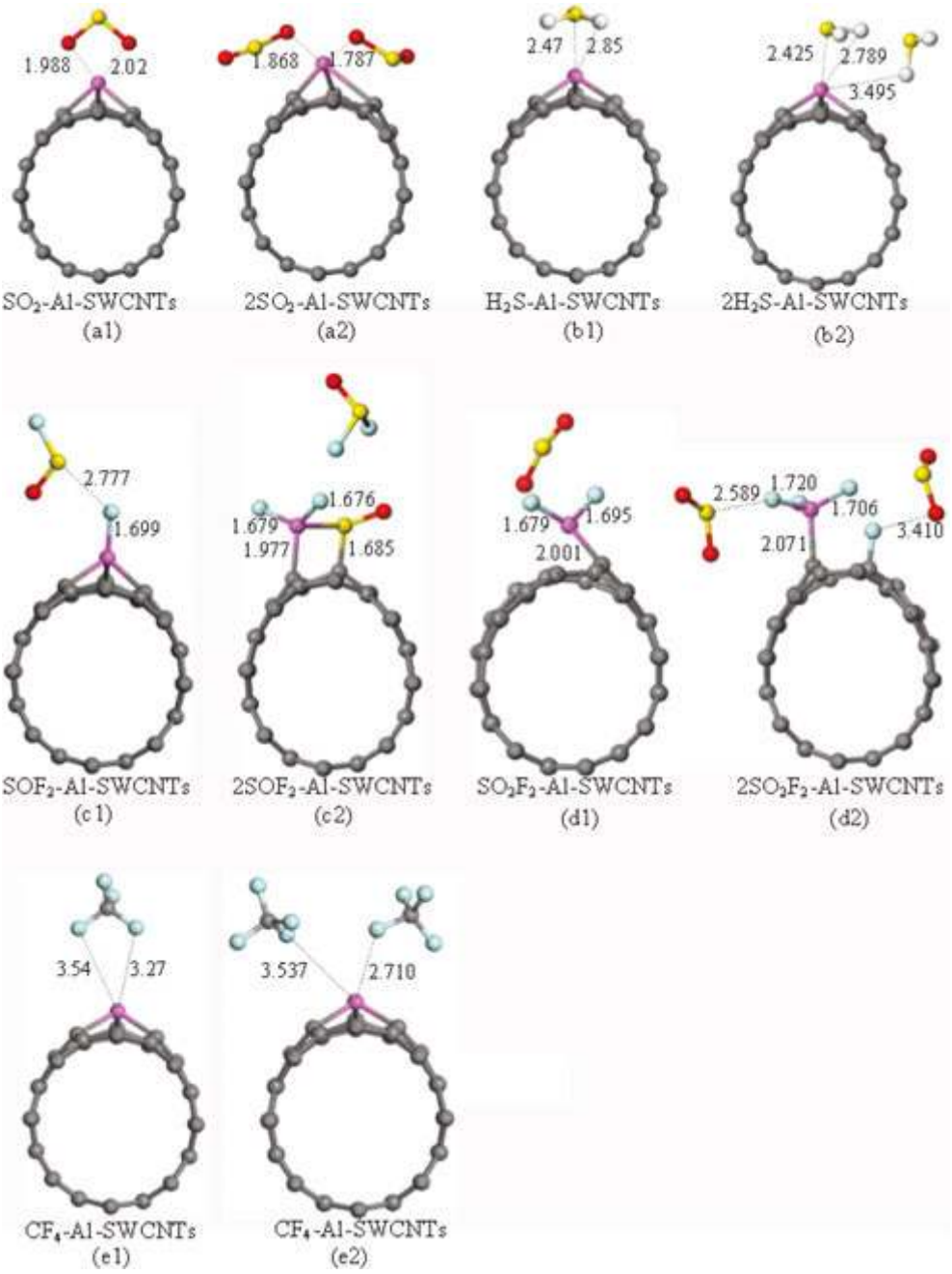

Figure 32. Most stable geometries of gas molecules interacting with Al-doped SWCNTs (distances in Å).

calculations. Al-SWCNTs can be considered a possible sensor material for the detection of H_2S owing to the adsorption energy and considerable charge transfer [32].

Based on the optimized adsorption structures of SOF_2 shown in **Figure 32c1** and **c2** and **Table 8** [32], two types of adsorption, namely single and double SOF_2 molecule adsorption, were outlined to analyze the adsorption capacity. From the relaxed structure of single SOF_2 molecule adsorption, the strong interaction between SOF_2 molecule and Al-SWCNTs decomposed the SOF_2 molecule to one SOF molecule and another fluorine atom [32]. The electronegative fluorine atom bonded to the Al atom through a strong chemical reaction, with the interaction distance of 1.699 Å. Meanwhile, the bond length from the produced SOF molecule to the fluorine atom was 2.777 Å, which indicated the decomposition of SOF_2 [32]. Upon double SOF_2 molecule adsorption, one of the SOF_2 molecules was adsorbed on the surface of Al-SWCNTs by chemisorption [38], whereas the other SOF_2 molecule was found far from the nanotube [32]. Two of the original Al—C bonds broke in the adsorption process. Then, two fluorine atoms of SOF_2 bonded to the Al atom [32].

As shown **Figure 32d1** and **d2** and **Table 8** [32], single and double SO_2F_2 molecules are adsorbed on the surface of Al-SWCNTs. After the structures have relaxed to reach the most steady state, only one original Al—C bond exists after the adsorption process. The other two bonds were broken because of the strong interaction between the F and Al atoms [32, 41]. Upon single SO_2F_2 molecule adsorption, two fluorine atoms separated from SO_2F_2 molecule and bonded to the Al atom, with bond lengths of 1.679 and 1.695 Å, respectively. Meanwhile, the produced SO_2 molecule was far from the surface of Al-SWCNTs. When another SO_2F_2 molecule was added, all of the fluorine atoms separated from the SO_2F_2 molecules. Three of the fluorine atoms bonded to the Al atom. The other fluorine atom bonded to the carbon atom of Al-SWCNTs. Both of the produced SO_2 molecules were far from the surface of Al-SWCNTs, with interactive distances of 2.589 and 3.410 Å, respectively. The weak interaction to the produced SO_2 might be because the Al-SWCNTs have reached saturated adsorption [32].

As shown in **Figure 32e1** and **e2** and **Table 8** [32], the CF_4 molecule was far from the surface of Al-SWCNTs, which was also ineffectively detected by other reported methods [42]. The nearest interaction distances reached 3.27 Å for single CF_4 molecule adsorption and 2.710 and 2.537 Å for double CF_4 molecule adsorption. The long interactions corresponded well with the low adsorption energies of −0.033 and −0.087 eV for single and double CF_4 molecule adsorption, respectively. Furthermore, weak physisorption was consistent with slight charge transfer [32].

2.5.3. The analysis of the density of states and frontier molecular orbital

In the previous section, we discussed the adsorption of single and double SF_6 decomposed gas molecules on Al-SWCNTs. We observed that the Al doping method showed good adsorption capacity for all of the SF_6 decomposed gas molecules, except for the CF_4 molecules, which indicated the possibility of detecting these decomposition components [32]. However, the detecting mechanism of Al-SWCNTs depends on its conductivity change after gas adsorption. The density of states (DOS) and frontier molecular orbitals were investigated to analyze the change of conductivity. The total electron DOS (TDOS) and local DOS (LDOS) were determined to investigate the influence of gas adsorption and to elucidate the electronic properties

http://dx.doi.org/10.5772/intechopen.68325

of Al-SWCNTs and molecule-Al-SWCNTs [32, 43], as shown in **Figure 33**. The highest occupied molecular orbital (HOMO) and lowest unoccupied molecular orbital (LUMO) upon molecule adsorption on the Al-doped SWCNTs are listed in **Table 9**. The corresponding diagrams of HOMO and LUMO are shown in **Figure 34** [32].

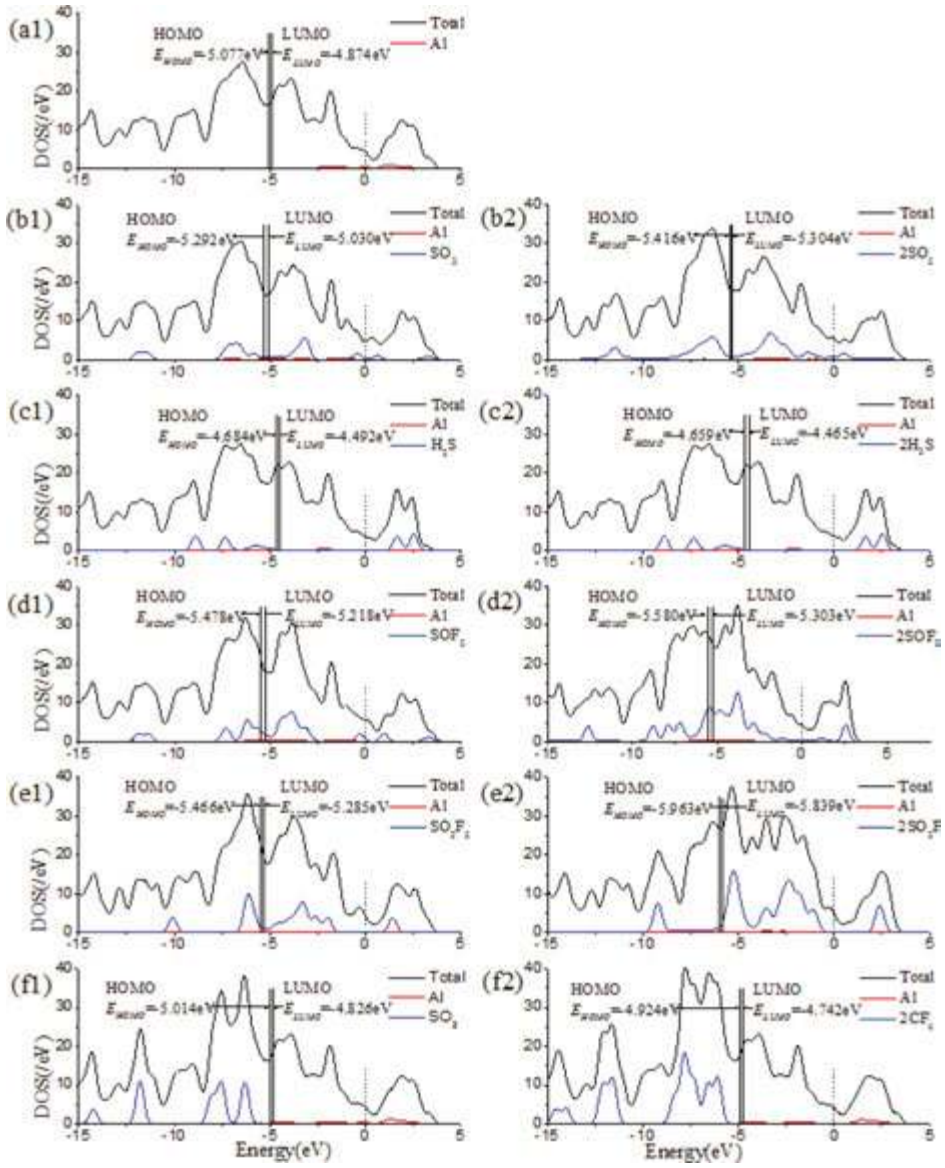

Figure 33. TDOS and LDOS of the Al-SWCNTs and molecule-Al-SWCNTs. Dashed and solid lines indicate the Fermi level and HOMO-LUMO, respectively.

System	EHOMO (eV)	ELUMO (eV)	Eg (eV)
Al-SWCNTs	−5.077	−4.874	0.203
SO_2-Al-SWCNTs	−5.292	−5.030	0.262
$2SO_2$-Al-SWCNTs	−5.416	−5.304	0.112
H_2S-Al-SWCNTs	−4.684	−4.492	0.192
$2H_2S$-Al-SWCNTs	−4.659	−4.465	0.194
SOF_2-Al-SWCNTs	−5.478	−5.218	0.260
$2SOF_2$-Al-SWCNTs	−5.580	−5.303	0.277
SO_2F_2-Al-SWCNTs	−5.466	−5.285	0.181
$2SO_2F_2$-Al-SWCNTs	−5.963	−5.839	0.124
CF_4-Al-SWCNTs	−5.014	−4.826	0.188
$2CF_4$-Al-SWCNTs	−4.924	−4.742	0.182

Table 9. HOMO and LUMO energies (E_{HOMO}, E_{LUMO}) and HOMO-LUMO energy gap (E_g).

Based on the DOS of SF_6 decomposition products before and after adsorption (**Figure 33**) [32], we observed that the LDOS of the Al atom had only a slight contribution to each TDOS. The changes of TDOS were mainly from the adsorbed molecules. Meanwhile, the various changes induced by different adsorbed molecules only provided the chance to detect the SF_6 decomposition products selectively [32].

Based on **Figure 33a1** [32], the TDOS of Al-SWCNTs was apparently distributed to all energy band areas, which reached 4.43 eV at the Fermi level. This finding indicated that Al-SWCNTs are still a good conductor after Al atom doping. The results are in accordance with other experiments on metal-doped materials [44]. **Figure 33a1** and **a2** shows the frontier molecular orbitals of Al-SWCNTs. In addition, the HOMO and LUMO were uniformly located on the Al-SWCNT surface. The HOMO and LUMO of the Al atom were mainly contributed by its *s* orbital. **Table 9** shows that E_{HOMO} and E_{LUMO} of Al-SWCNTs were −5.077 and −4.874 eV, respectively, and E_g was 0.203 eV [32].

The TDOS for SO_2 molecules adsorbed on Al-SWCNTs is shown in **Figure 33b1** and **b2** [32]. When one SO_2 molecule was adsorbed on the surface of Al-SWCNTs, the TDOS slightly increased at and under the Fermi level compared with that of pristine Al-SWCNTs. As shown in **Figures 22b2** and **33b1**, the HOMO and LUMO were entirely located on the carbon atoms upon single SO_2 adsorption. The HOMO energy shifted from −5.077 to −5.292 eV, and the LUMO energy shifted to −5.030 eV in the pristine Al-SWCNTs. E_g was slightly increased to 0.262 eV compared with that of Al-SWCNTs. Upon the second SO_2 molecule adsorption, the TDOS further increased with respect to that of the single molecule adsorption [32]. In addition, E_g decreased to 0.112 eV when the HOMO and LUMO are mainly located on SO_2 molecules and carbon atoms. Considering the increased TDOS and decreased E_g, the conductivity of Al-SWCNTs tended to increase with SO_2 adsorption [20].

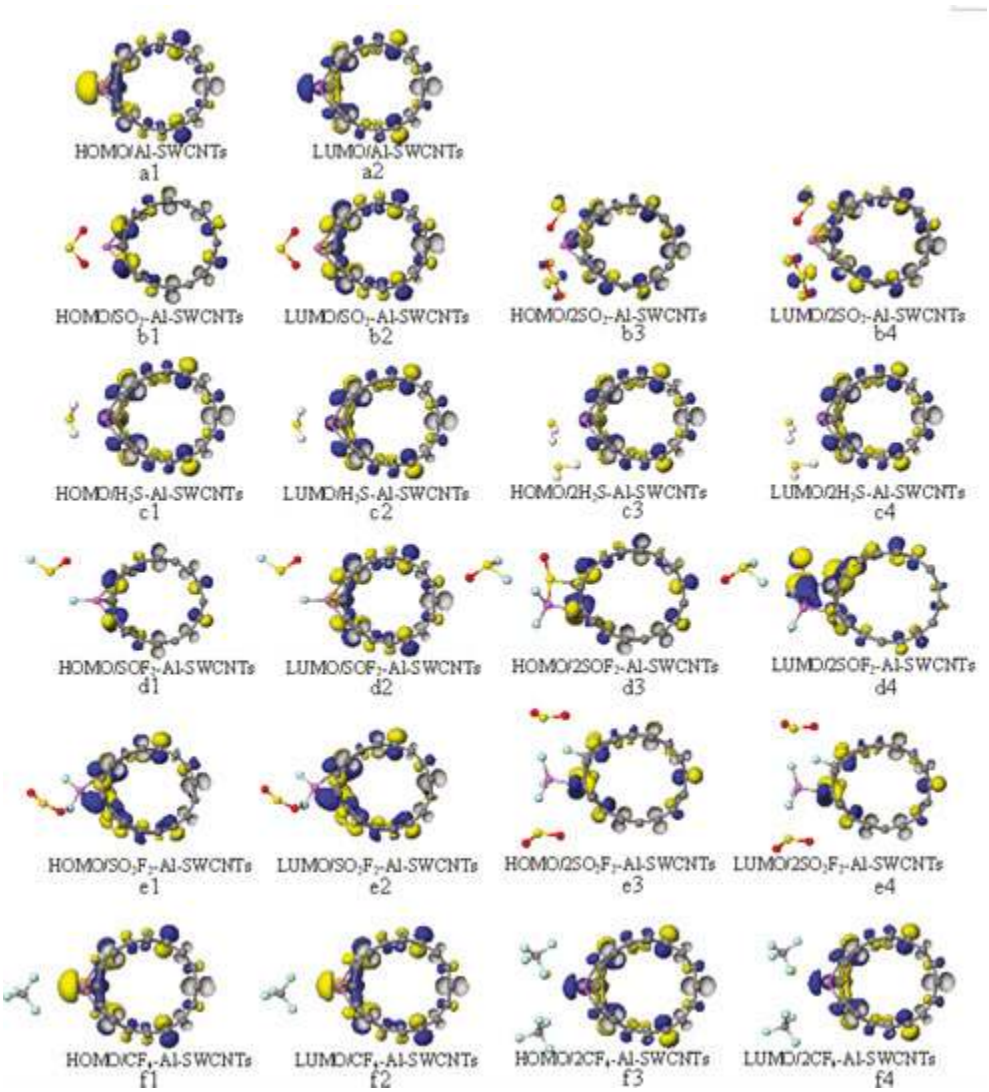

Figure 34. HOMO and LUMO orbitals on Al-SWCNTs and molecule-Al-SWCNTs. From top to bottom: (a1)–(f1) and (b3)–(f3) represent the HOMO orbitals, and (a2)–(f2) and (b4)–(f4) represent the LUMO orbitals.

As shown in **Figure 33c1** and **c2**, the LDOS induced by the H_2S molecules was partly located above the Fermi level, which contributed to the TDOS above the Fermi level. The change of the HOMO and LUMO energies slightly shifted to the right side. E_g for the single and double H_2S molecule adsorption was 0.192and 0.194 eV, respectively, and was smaller than that of pristine Al-SWCNTs. As shown in **Figure 33c1–c4**, the HOMO and LUMO were still

distributed on pristine Al-SWCNTs. In general, the interaction between the H_2S molecules and Al-SWCNTs was favorable and enhanced the conductivity of Al-SWCNTs.

Based on the SOF_2 molecules adsorbed on Al-SWCNTs shown in **Figure 33d1** and **d2**, the LDOS of SOF_2 molecules was mainly below the Fermi level. Herein, the TDOS at the Fermi level was slightly changed compared with that of pristine Al-SWCNTs. However, E_g evidently increased to 0.260 eV for single SOF_2 adsorption and further increased to 0.277 eV when another SOF_2 molecule was adsorbed (**Table 9**). As shown in **Figure 33d1–d4**, the HOMO and LUMO orbitals were distributed on the carbon atoms for single SOF_2 molecule adsorption [32]. Meanwhile, the distribution of the molecular orbital for double SOF_2 molecule adsorption was different, where the HOMO orbital was located on the carbon atoms and the LUMO orbital was located on all of the Al-SWCNTs [32]. Based on the previously presented analysis, conductivity might decrease to a certain extent [32].

When one SO_2F_2 molecule was adsorbed on Al-SWCNTs, the TDOS decreased around the Fermi level (**Figure 33e1**). The LDOS of SO_2F_2 was primarily below the HOMO energy and above the LUMO energy, with the decrease in E_g to 0.181 eV. When the other SO_2F_2 molecule was adsorbed, the TDOS continued to decrease above the Fermi level. With LDOS induced by double SO_2F_2 molecules, we observed that the TDOS distinctly increased above the LUMO energy (see **Figure 33e2**). The value of E_g decreased to 0.124 eV, which facilitated electron conduction between molecular orbitals. As shown in **Figure 33e1–e4**, the HOMO and LUMO orbitals were totally shifted to the carbon atoms after SO_2F_2 adsorption. The strong bond energy between the Al and F atoms seemed to weaken the electron conduction ability among atoms other than carbon [32].

As mentioned previously, the interaction between CF_4 molecules and Al-SWCNTs was weak, resulting in a limited influence of the CF_4 molecules [45]. The LDOS of CF_4 was below the HOMO energy shown in **Figure 33f1** and **f2** [32]. Meanwhile, the TDOS around the Fermi level remains unchanged. E_g (0.188 and 0.182 eV) was slightly smaller than that of pristine Al-SWCNTs. Similarly, the HOMO and LUMO orbitals were almost the same as that of Al-SWCNTs before CF_4 adsorption. Therefore, we conclude that the conductivity of Al-SWCNTs would not change upon CF_4 adsorption.

2.5.4. Summary: gas adsorption on Al-SWCNT

In this study, we analyzed the adsorption of the gases produced by SF_6 decomposition (i.e., SO_2, H_2S, SOF_2, SO_2F_2 and CF_4) on the Al-SWCNT surface using GGA and DFT calculations and considering different sites to determine the most stable structures. In addition, multiple-molecule adsorption was calculated for SF_6 decomposition products to analyze the various changes of conductivity induced by adsorption [32].

The results indicated that the SO_2 molecules were physically adsorbed on Al-SWCNTs. This interaction increased the TDOS and decreased the E_g, which increased the conductivity of the adsorption system [32]. Upon H_2S adsorption, considerable E_{ads} resulted in well-adsorbed H_2S molecules on the surface of Al-SWCNTs. However, the change of conductivity was not evident based on the analyses of DOS and frontier molecular orbital. The SOF_2 and SO_2F_2 molecules were

chemisorbed on the surface of Al-SWCNTs because of the strong interaction between the Al and F atoms. The conductivity of SOF_2 adsorbed on Al-SWCNTs decreased to a certain extent as a result of the increase in E_g and decrease in TDOS around the Fermi level [32]. For SO_2F_2 adsorption, although the TDOS around the Fermi level showed a slight decrease, the evident decrease in E_g indicated that conductivity might be enhanced upon SO_2F_2 adsorption. The calculation results showed that conductivity is unchanged during CF_4 adsorption mainly because the interaction between Al-SWCNTs and CF_4 molecules was weak to induce electron redistribution [32].

In summary, Al atom doping method is potentially an effective technique to adsorb the gases produced by SF_6 decomposition. Through the different changes in conductivity induced by molecule adsorption, the selective detection of each type of SF_6 decomposed gas was achieved. We hope that this innovative study would further accelerate research on the mechanism of metal doping methods in detection of gases from SF_6 decomposition [32].

2.6. Gas-sensing properties of Pt-SWCNTs to SO_2, H_2S

2.6.1. Structural parameters of intrinsic Pt-SWCNT

The radius of Pt atom is 0.183 nm, which is greater than that of C atom (0.070 nm). Thus, Pt is highlighted on the CNT surface as shown in **Figure 35**. The bond lengths between Pt atom and three adjacent C atoms changed from 0.142 nm to 0.199, 0.199 and 0.189 nm for Pt-C1, Pt-C2 and Pt-C3, respectively [16]. These results are consistent with Refs. [16, 46].

Figure 35. Geometric structures of Pt-doped SWCNTs after optimization. The structural parameters are shown as Å.

2.6.2. The analysis of gas adsorption structure

Pt is not only a sensing element of Pt-SWCNTs, but also an active site. Strong interaction with gas molecules adsorbed on the surface results in deformation of Pt-SWCNTs and elongation of Pt-C bond. The full geometric optimization of the Pt-SWCNTs and SO_2 adsorption model is shown in **Figure 36**. An oxygen atom O1 points to Pt, in which the distances of Pt-O1 and Pt-S are 0.212 and 0.245 nm, respectively.

The reaction adsorption energy for SO_2 adsorption is −1.225 eV, which denotes an exothermic and spontaneous reaction. According to Mulliken charge population analysis shown in **Table 10**, SWCNTs of Pt-SWCNTs have 0.147 positive charge, and Pt has 0.147 negative charge before adsorption. After the adsorption process, SWCNTs have 0.509 positive charge, whereas Pt has 0.116 negative charge. SO_2 obtains 0.301 electrons during the adsorption reaction [16]. Charge variation (ΔQ_{SWCNTs}, ΔQ_{Pt}) of SWCNTs and Pt is 0.362 and 0.031, respectively. Therefore, SO_2 obtains electrons mainly from SWCNTs, whereas Pt exhibits a small charge change.

As shown in **Table 10** [16], Mulliken charge analysis shows that H_2S donates 0.285 electrons. Pt and SWCNTs, respectively, have 0.019 and 0.266 electrons after H_2S is adsorbed on Pt-SWCNTs. A large number of electron transformations convert Pt-SWCNTs from *p*-type to *n*-type.

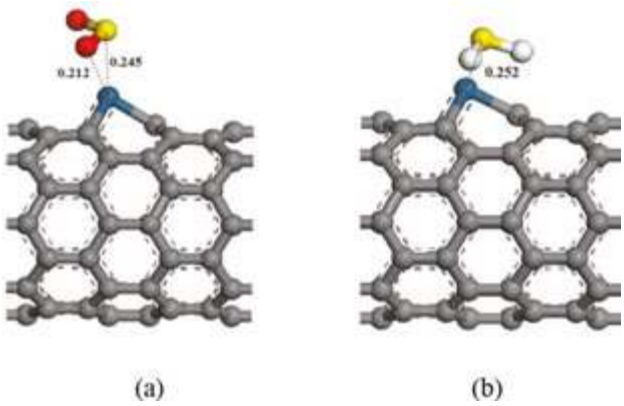

Figure 36. Structural model of the SO_2-Pt-SWCNT adsorptive system. (a) Front view; (b) side view.

System	Q_{SWCNTs}/e	Q_{Pt}/e	Q_{gas}/e	ΔQ_{SWCNTs}/e	ΔQ_{Pt}/e
Pt-SWCNTs	0.147	−0.147			
SO_2-Pt-SWCNTs	0.509	−0.116	-0.393	0.362	0.031
H_2S-Pt-SWCNTs	−0.019	−0.266	0.285	−0.166	−0.119

Table 10. Electrical structure parameters of the adsorption structures.

2.6.3. The analysis of the density of states and frontier molecular orbital

The transfer of a large number of electrons during adsorption causes the redistribution of system charges. The density of states (DOS) near Fermi level appears impure state, and the DOS between HOMO and LUMO changes. **Figure 37** shows that these impure states are caused by SO_2 adsorption. The *p* orbitals of S and O atoms have significant influence on the frontier orbital of the adsorption system, which changes the HOMO and LUMO orbital formation, thereby causing the change in DOS. **Figure 38a** shows that the *p* orbitals of C1 and C3 form σ bond with S, and in **Figure 38b**, the *d* orbitals of Pt and the *p* orbitals of S are hybridized [16]. The frontier orbital energy gap E_g of the system is 0.283 eV after adsorbing SO_2, which is reduced by 0.049 eV compared with the non-adsorbed SO_2 [16]. This observation is beneficial for the transfer of electrons between the HOMO and LUMO, thereby enhancing conductivity [16].

SO_2 adsorption on the surface of Pt-SWCNTs has large adsorption energy and can form a stable structure. The *p*-type Pt-SWCNTs [16, 47] donate electrons and increase hole carriers, thereby reducing the frontier orbital energy, diminishing energy gap E_g and enhancing conductivity. Pt-SWCNTs are highly responsive to SO_2 [16].

The adsorption reaction of Pt-SWCNTs and H_2S is also exothermic, with E_b of −0.977 eV. The frontier orbital energy difference $E_{H\text{-}L}$ = 4.438 eV and $E_{L\text{-}H}$ = 1.519 eV, so H_2S provides electrons to Pt-SWCNTs in this reaction. H_2S-Pt-SWCNT frontier orbitals concentrate on Pt-SWCNTs, and H_2S is not involved in the composition of HOMO and LUMO orbitals shown in **Figure 39**. **Figure 40** shows that DOS of H_2S is not distributed between HOMO and LUMO. DOS near the Fermi level is basically the same with Pt-SWCNTs, which is consistent with the results of frontier orbitals.

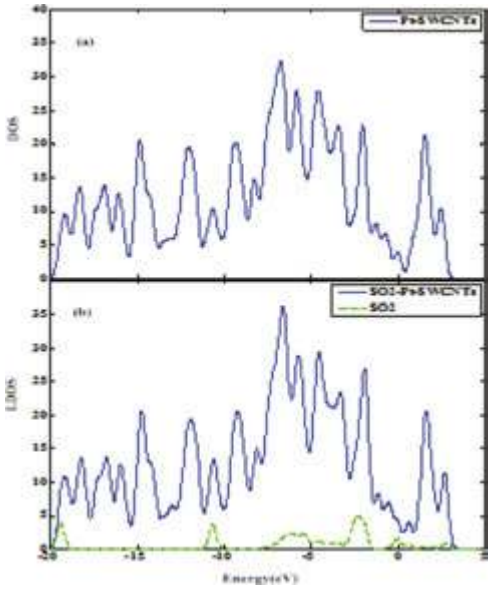

Figure 37. Density of states of Pt-SWCNTs before and after SO_2 adsorption (Fermi level is 0 eV).

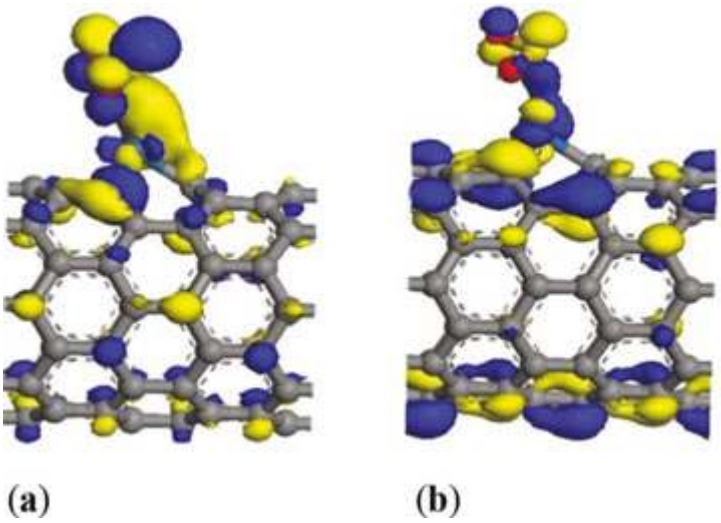

Figure 38. Frontier orbital energy level of SO_2-Pt-SWCNTs. (a) HOMO (−5.208 eV); (b) LUMO (−4.923 eV).

2.6.4. Summary: gas adsorption on Pt-SWCNTs

In this study, adsorptions of three gases on the surface of Pt-SWCNTs were calculated based on DFT [16]. The gas-sensing properties of Pt-SWCNTs were assessed according to the changes in adsorption energy, geometric structure and electronic structure during adsorption. The main conclusions are as follows [16]:

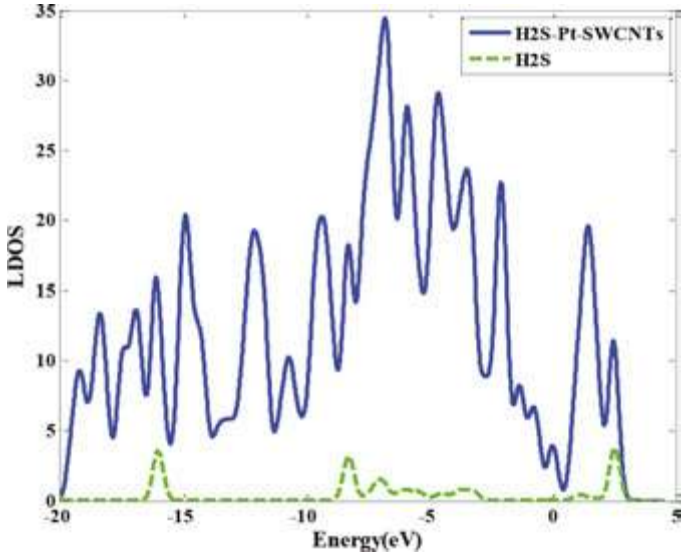

Figure 39. Frontier orbital energy level of H_2S-Pt-SWCNTs. (a) HOMO (−4.425 eV); (b) LUMO (−4.142 eV).

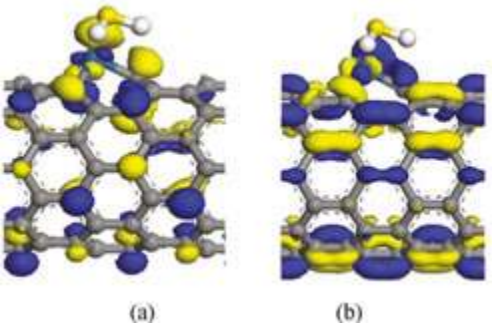

Figure 40. Partial DOS of H_2S-Pt-SWCNTs.

The three adsorption reactions are exothermic and spontaneous.

The adsorption energy of the reaction between Pt-SWCNTs and SO_2 is large, and numerous electrons are transferred from CNTs to the target gases [16]. The frontier orbital energies (E_{HOMO} and E_{LUMO}) and E_g decrease, and the electrical conductivity of Pt-SWCNTs is enhanced. Pt-SWCNTs have high sensitivity to SO_2 [16].

H_2S is reduced when reacted with Pt-SWCNTs and provide a large number of electrons, thereby converting CNTs from *p*-type to *n*-type. The frontier orbital energies increase, whereas E_g decreases, thereby enhancing conductivity [16].

Results of the theoretical calculation show that Pt-SWCNTs can respond to the three gases [16]. The electrical characteristics of Pt-SWCNTs show different degrees of changes after adsorption of the test gases. As SO_2 is adsorbed on Pt-SWCNTs, CNT loses electrons, hole carriers are increased and conductivity is enhanced [16]. As H_2S is adsorbed on the surface of CNTs, Pt-SWCNTs receive a large number of electrons and transforms from *p*-type into *n*-type. The conductivity of Pt-SWCNT is also enhanced [16]. Comparing their adsorption energies and charge transformations, the sensitivity of SO_2 is higher than that of H_2S for Pt-SWCNTs [16]. Therefore, Pt-SWCNTs can be used for fabricating gas sensors in detecting SO_2 and H_2S.

2.7. Gas-sensing properties of Au-SWCNTs to SO_2, H_2S

2.7.1. Structural parameters of intrinsic Au-SWCNTs

The radius of the Au atom is significantly greater than that of the C atom; thus, the Au atom of Au-SWCNT is highlighted on the nanotube surface shown in **Figure 41** [48]. The bond lengths between the Au atom and the three adjacent C atoms are 0.207 (Au—C1), 0.208 (Au—C2) and 0.196 nm (Au—C3). Compared with the C—C bond length of the intrinsic structure, the Au—C bond lengths are elongated by 38, 38 and 46%, respectively [48].

2.7.2. The analysis of gas adsorption structure

The adsorption structures of the gas molecules adsorbed by Au-SWCNT in different initial positions were calculated. We chose two initial positions that are parallel to the nanotube

Figure 41. Structural model of Au-SWCNT.

axis and three initial positions that are perpendicular to the nanotube axis. The initial positions were optimized in the geometrical structure [48]. During observation of the optimized structures, the stable adsorption structure of H_2S is the S atom located above the center of the ring that contains Au—C1—C2 [48]. Two main stable adsorption structures of SO_2 exist. One is the S atom located above the Au—C bond and an O atom above the center of the ring that contains Au—C1—C2; another is the S atom located above the center of the ring [48]. SO_2 that is parallel to the axis, and two O atoms above the Au and C atom, respectively. Comparing the two structures, the former is more stable. The most stable adsorption structure is shown in **Figure 42**. **Table 11** lists the adsorption energy and the structural parameter [48].

The adsorption energy of SO_2 is −1.258 eV, which indicates that the adsorption is exothermic and spontaneous. After SO_2 is adsorbed to Au-SWCNT, the structures of Au-SWCNT (**Table 11**) and SO_2 (**Figure 42**) changed [48]. Au—C1 and Au—C2 are elongated by 3.38 and 4.33%, respectively. Moreover, S—O is also elongated. The modified element of CNT is the sensing element and the active site of the modified CNT [48]. The adsorption partially depends

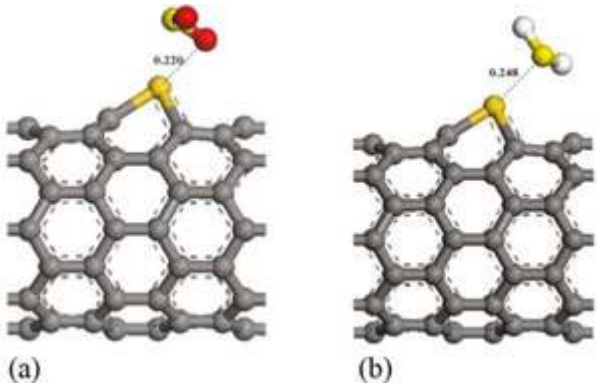

Figure 42. Front and side views of the stable structural model of (a) SO_2-Au-SWCNT and (b) H_2S-Au-SWCNT.

Type	SO_2	H_2S
$d_{Au—C1}$/nm	0.214	0.217
$d_{Au—C2}$/nm	0.217	0.218
$d_{Au—C3}$/nm	0.195	0.195
E_b/eV	−1.258	−1.317

Table 11. Adsorption energy and the structural parameter.

on the interaction between the gas molecule and the sensing element. The strong attraction in the adsorption of SO_2 and Au-SWCNT caused the structural change of Au-SWCNT [48]. The Au—C bond length increased, the bond energy decreased, and the bond activity strengthened. Simultaneously, the electrons are transferred to SO_2, and the excess electrons fill the anti-bonding orbits of SO_2. The increase in repulsion results in a change in the S—O bond length from 0.148 nm to 0.150 and 0.160 nm [48].

The adsorption between H_2S and Au-SWCNT is also exothermic, and the adsorption energy is −1.317 eV. Compared with SO_2, the interaction is slightly stronger. Au—C1 and Au—C2 are elongated by 4.83 and 4.81%, respectively [48].

From the above analysis, Au-SWCNT has a strong adsorption with SO_2 and H_2S, and their adsorption energies are greater than 1 eV. The adsorption reaction can occur at room temperature and the strong interaction changes the geometric structure of the adsorption system [48].

2.7.3. The analysis of the density of states and frontier molecular orbital

In **Table 12** [48], the LUMO of SO_2 was approximated to the HOMO of Au-SWCNT, and the difference of the two orbital energies is only 0.065 eV. The electron of Au-SWCNT only needs to cross a very low energy barrier to transfer to SO_2. In turn, the electron needs to cross a 3.603 eV energy barrier for the electron of SO_2 to transfer to Au-SWCNT, but this process is

System	E_{HOMO}/eV	E_{LUMO}/eV	$E_{L\text{-}H}$/eV	$E_{H\text{-}L}$/eV			
Au-SWCNT	−4.795	−4.585					
SO_2	−8.188	−4.860	3.603	0.065			
H_2S	−5.889	−0.264	1.304	4.531			
System	E_g/eV	Q_{SWCNT}/e	Q_{Au}/e	Q_{gas}/e	ΔE_g/eV	ΔQ_{SWCNT}/e	ΔQ_{Au}/e
Au-SWCNT	0.210	0.070	−0.070				
SO_2-Au-SWCNT	0.183	0.339	−0.038	−0.301	−0.027	0.269	0.032
H_2S-Au-SWCNT	0.245	−0.106	−0.180	0.286	0.035	−0.176	−0.110

Table 12. Electrical structure parameters of the adsorption structures.

more difficult [48]. Thus, the electrons transfer from Au-SWCNT to SO_2 during adsorption. According to Mulliken charge population, SO_2 obtains 0.301 electrons during the adsorption reaction. SWCNT and Au lose 0.269 and 0.032 electrons, respectively. Au has a key role in the adsorption reaction. **Figure 43** shows the three-dimensional plot of the deformation electron density of SO_2-Au-SWCNT [48]. The range is from −0.976 to 0.345 e/nm. The negative value denotes loss of electrons and a decrease in the electron density. The positive value denotes gain of electrons and an increase in the electron density. As seen from the plot, the charge of Au-SWCNT was redistributed after it adsorbed SO_2. SO_2 obtained electrons, whereas Au-SWCNT lost electrons. Correspondingly, the HOMO and LUMO move toward the nuclear and the orbital energy decreases. Au-SWCNT is a p-type semiconductor. The transferred electrons increased the electron holes and simultaneously increased the carriers, enhanced the conductivity, and decreased the frontier orbital energy gap (**Table 12**) [48].

To clarify further the adsorption processes of SO_2, the partial density of states (PDOSs) of the S, O and Au atoms are shown in **Figure 44** [48]. Their PDOSs overlap in the energy region of −10 to −2.5 eV. In this area, the d orbitals of Au, the p orbitals of the S and O atoms are hybridized as the molecular orbitals of the system. In addition, the d orbitals of Au and the p orbitals of S effectively overlap at the Fermi energy (−2.5 eV to 2.5 eV), which strengthens the interaction between the two atoms. The hybridized orbitals at the Fermi level introduce an impurity level and are conducive for the electrons to transfer to SO_2 from Au-SWCNT [48].

Based on the changes in the electronic structure of adsorption system, a significant amount of electrons is transferred in the adsorption process between SO_2 and Au-SWCNT. Au-SWCNT loses electrons, the frontier orbital energy gap decreases, and the conductivity is enhanced. In conclusion, the Au-SWCNT has a good sensitivity to SO_2 and can be used to detect SO_2 gas based on the changes in its conductivity [48].

The S of H_2S is at the lowest valence state. It has a strong reducibility and can provide electrons during the reaction process. In contrast to SO_2, the HOMO of H_2S was approximated to the

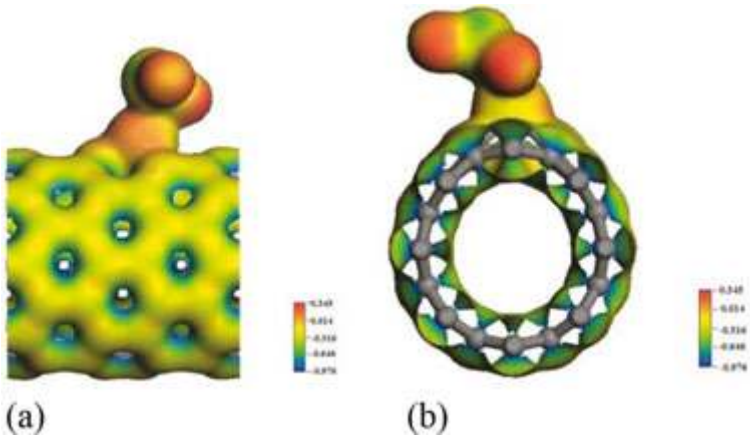

Figure 43. Deformation electron density of SO_2-Au-SWCNT. (a) Front view; (b) side view.

http://dx.doi.org/10.5772/intechopen.68325

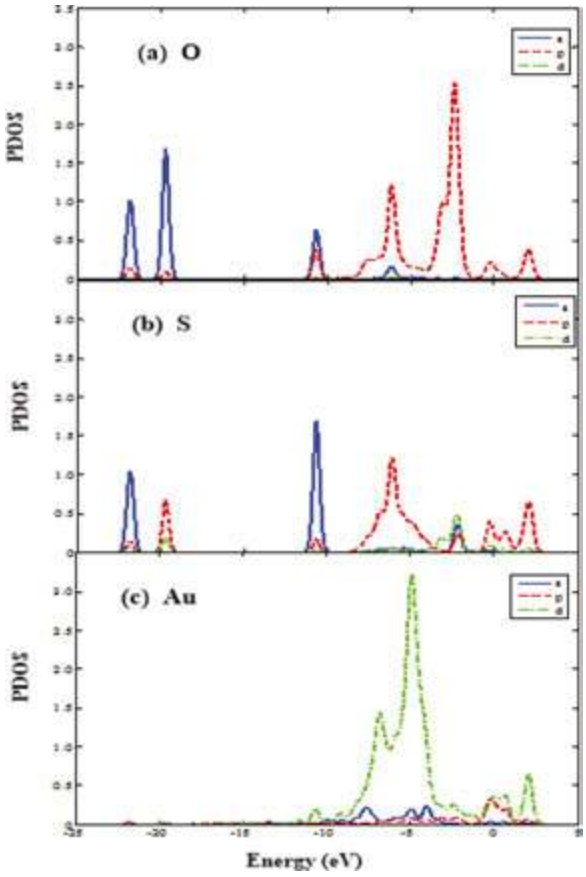

Figure 44. PDOS of SO_2-Au-SWCNT. (a) O; (b) S; (c) Au.

LUMO of Au-SWCNT, and the difference of the energy is only 1.304 eV. Therefore, the electrons of H_2S are easily transferred to Au-SWCNT. Transferring the electrons of Au-SWCNT to H_2S is difficult. Thus, when H_2S was adsorbed to Au-SWCNT, the electrons were transferred from H_2S to Au-SWCNT [48]. According to the Mulliken charge population, the H_2S molecule loses 0.286 electrons. The SWCNT and the Au atom obtain 0.176 and 0.110 electrons, respectively. The three-dimensional plot of the deformation electron density of H_2S-Au-SWCNT is shown on **Figure 45** [48]. The range is −1.172 to 0.320 e/nm. The charges of Au-SWCNT and the adsorbed H_2S are redistributed, H_2S loses electrons and Au-SWCNT gains electrons. Correspondingly, the HOMO and LUMO of Au-SWCNT move away from the nucleus and the orbital energy increases. The transferred electrons decreased the number of electron holes, along with the number of carriers and the conductivity. The frontier orbital energy gap also increased (**Table 12**) [48].

When observing the PDOSs of the adsorption system shown in **Figure 46** [48], which is similar to that of SO_2, the PDOSs of Au in Au-SWCNT and S in H_2S are overlapping. The d orbitals

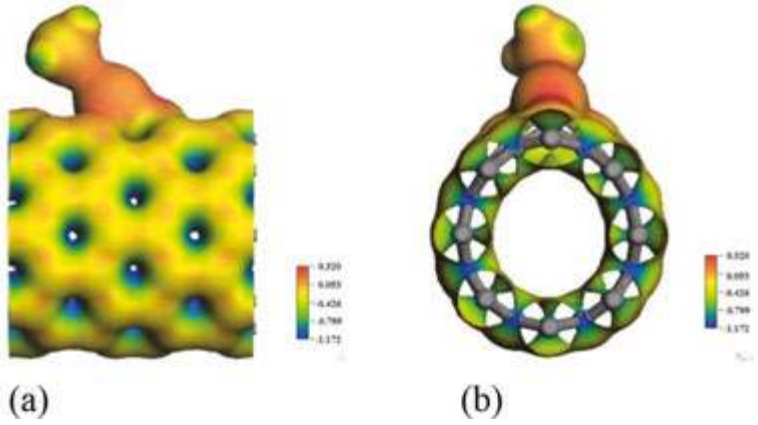

Figure 45. Deformation electron density of H_2S-Au-SWCNT. (a) Front view; (b) side view.

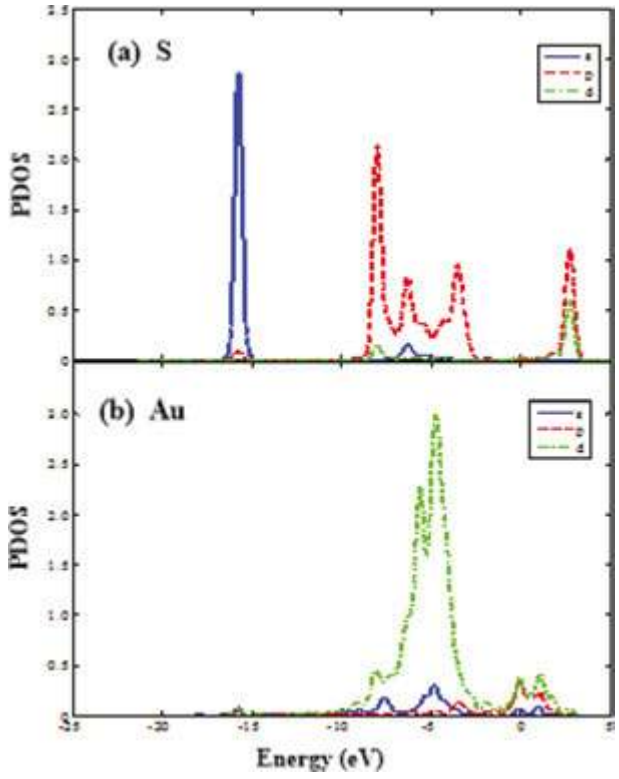

Figure 46. PDOS of H_2S-Au-SWCNT. (a) S; (b) Au.

of Au and the p orbitals of the S atom are hybridized, which is advantageous to the electron transfer and strengthens the interaction between the adsorbed H_2S and Au-SWCNT.

Therefore, Au-SWCNT has a good sensitivity to H_2S, and H_2S can be effectively adsorbed on the surface of Au-SWCNT [48]. When the Au-SWCNT acquired electrons, the frontier orbital energy gap increased, and the conductivity decreased. Hence, Au-SWCNT can be used to detect H_2S [48].

2.7.4. Summary: gas adsorption on Al-SWCNTs

In this study, the adsorption reactions of the two gases on the surface of Au-SWCNT were calculated by DFT, and the sensitivity of Au-SWCNT to the two gases was analyzed [48].

The main conclusions of this study are as follows:

The reactions between the two gases and Au-SWCNT are both exothermic, and the adsorption energies are huge. The interaction between the gas molecule and the nanotubes caused the structure to change, for example, Au─C elongate [48].

During the adsorption process of SO_2, SO_2 acquires electrons and Au-SWCNT loses electrons. The frontier orbital energy gap decreases, and the electrical conductivity of p-type Au-SWCNT is enhanced.

During the adsorption process of H_2S, H_2S loses electrons and Au-SWCNT acquires electrons. The frontier orbital energy gap increases, and the electrical conductivity of p-type Au-SWCNTs decreases.

The theoretical calculation results show that Au-SWCNT has a good sensitivity to both SO_2 and H_2S [48]. The conductivity changes caused by the two gases are inversely proportional. Thus, Au-SWCNT can be used to detect SO_2 and H_2S [48]. This conclusion is helpful to the development of CNT-based gas sensors and provides a theoretical basis for developing Au-SWCNT-based gas sensor [48].

Acknowledgements

Parts of this chapter are reproduced from Refs. [11, 31, 45] with Elsevier's, and from Ref. [32] with Springer's permission.

Author details

Xiaoxing Zhang*, Song Xiao, Ju Tang and Cheng Pan

*Address all correspondence to: xiaoxing.zhang@outlook.com

School of Electrical Engineering, Wuhan University, Wuhan, China

References

[1] Iijima S. Helical microtubules of graphitic carbon. Nature. 1991;**354:**56-58

[2] Hone J, Fischer JE. Quantized phonon spectrum of single-wall carbon nanotubes. Science. 2000;**289**:1730-1733

[3] Krishnan A, Dujardin E, Ebbesen TW, Yianilos PN, Treacy MMJ. Young's modulus of single-walled nanotubes. Physical Review B. 1998;**58**:14013

[4] Ebbesen TW, Ajayan PM. Large-scale synthesis of carbon nanotubes. Nature. 1992;**358**:220-222

[5] Lin X, Wang XK, Dravid VP, Chang RPH, Ketterson J.B. Large scale synthesis of single-shell carbon nanotubes. Applied Physics Letters. 1994;**64:**181-183

[6] Yan Y, Wang WQ, Zhang LX. Dynamical behaviors of fluid-conveyed multi-walled carbon nanotubes. International Journal of Modern Physics B. 2009;**33**:1430-1440

[7] Perdew JP, Burke K, Ernzerhof M. Generalized gradient approximation made simple. [Physical Review Letters 1996;**77:**3865], Physical Review Letters, 1997;**78:**1396

[8] Zhang X, Meng F, Wang Z, Li J. Gas-sensing simulation of single-walled carbon nanotubes applied to detect gas decomposition products of SF6 in PD, In: 2011 Electrical Insulation Conference (EIC). 2011, pp. 132-135

[9] Zhao Q, Nardelli MB, Lu W, Bernholc J. Carbon nanotubes-metal cluster composites: A new road to chemical sensors. Nano Letters. 5:847-851, Nano Letters. 2005;**5:**847-851

[10] Bulat FA, Chamorro E, Fuentealba P, Toro-Labbé A. Condensation of frontier molecular orbital Fukui functions. The Journal of Physical Chemistry A. 2004;**108**:342-349

[11] Zhang X, Gui Y, Xiao H, Zhang Y. Analysis of adsorption properties of typical partial discharge gases on Ni-SWCNTs using density functional theory. Applied Surface Science. 2016;**379:**47-54

[12] Banerjee S, Hemraj-Benny T, Wong S.S. Covalent surface chemistry of single-walled carbon nanotubes. Advanced Materials. 2005;**17:**17-29

[13] Felten A, Bittencourt C, Pireaux JJ, Lier GV, Charlier J.C. Radio-frequency plasma functionalization of carbon nanotubes surface O_2, NH_3, and CF_4 treatments. Journal of Applied Physics. 2005;**98:**074308-074308-074309

[14] Valentini L, Puglia D, Armentano I, Kenny JM. Sidewall functionalization of single-walled carbon nanotubes through CF_4 plasma treatment and subsequent reaction with aliphatic amines. Chemical Physics Letters. 2005;**403:**385-389

[15] Shulga YM, Tien TC, Huang CC, Lo SC, Muradyan VE, Polyakova NV, Ling YC, Loutfy RO, Moravsky AP. XPS study of fluorinated carbon multi-walled nanotubes. Journal of Electron Spectroscopy & Related Phenomena. 2007;**160:**22-28

[16] Zhang X, Dai Z, Wei L, Liang N, Wu X. Theoretical calculation of the gas-sensing properties of Pt-decorated carbon nanotubes. Sensors. 2013;**13:**15159-15171

[17] Wang R, Zhang D, Sun W, Han Z, Liu C. A novel aluminum-doped carbon nanotubes sensor for carbon monoxide. Journal of Molecular Structure: THEOCHEM. 2007;**806:**93-97

[18] Yeung CS, Liu LV, Wang YA. Adsorption of small gas molecules onto Pt-doped single-walled carbon nanotubes. The Journal of Physical Chemistry C. 2008;**112:**7401-7411

[19] Zhang X, Dai Z, Wei L, Liang N, Wu X. Theoretical calculation of the gas-sensing properties of Pt-decorated carbon nanotubes. Sensors. 2013;**13:**15159-15171

[20] Zhou X, Tian WQ, Wang X-L. Adsorption sensitivity of Pd-doped SWCNTs to small gas molecules. Sensors and Actuators B: Chemical. 2010;**151:**56-64

[21] Zhang X, Dai Z, Chen Q, Tang J. A DFT study of SO_2 and H_2S gas adsorption on Au-doped single-walled carbon nanotubes. Physica Scripta. 2014;**89:**065803

[22] Star A, Joshi V, Skarupo S, Thomas D, Gabriel J-CP. Gas sensor array based on metal-decorated carbon nanotubes. The Journal of Physical Chemistry B. 2006;**110:**21014-21020

[23] López-Corral I, Germán E, Volpe MA, Brizuela GP, Juan A. Tight-binding study of hydrogen adsorption on palladium decorated graphene and carbon nanotubes. International Journal of Hydrogen Energy. 2010;**35:**2377-2384

[24] Byl O, Kondratyuk P, Forth ST, FitzGerald SA, Chen L, Johnson JK, Yates JT. Adsorption of CF4 on the internal and external surfaces of opened single-walled carbon nanotubes: A vibrational spectroscopy study. Journal of the American Chemical Society. 2003;**125:**5889-5896

[25] O'Boyle NM, Tenderholt AL, Langner KM. cclib: A library for package-independent computational chemistry algorithms. Journal of Computational Chemistry. 2008;**29:**839-845

[26] Camilli G, Chapman JJ. Gaseous insulation for high-voltage apparatus, American Institute of Electrical Engineers. Transactions of the American Institute of Electrical Engineers. 1947;**66:**1463-1470

[27] Robin-Jouan P, Yousfi M. New breakdown electric field calculation for SF_6 high voltage circuit breaker applications. Plasma Science and Technology. 2007;**9:**690

[28] Pannopard P, Khongpracha P, Probst M, Limtrakul J. Gas sensing properties of platinum derivatives of single-walled carbon nanotubes: A DFT analysis. Journal of Molecular Graphics and Modelling. 2009;**28:**62-69

[29] Bak S-M, Kim K-H, Lee C-W, Kim K-B. Mesoporous nickel/carbon nanotube hybrid material prepared by electroless deposition. Journal of Materials Chemistry. 2011;**21:**1984-1990

[30] Yu S, Yi W. Single-walled carbon nanotubes as a chemical sensor for SO_2 detection. IEEE Transactions on Nanotechnology. 2007;**6;**545-548

[31] Zhang X, Gui Y, Dai Z. A simulation of Pd-doped SWCNTs used to detect SF_6 decomposition components under partial discharge. Applied Surface Science. 2014;**315:**196-202

[32] Zhang X, Gui Y, Dai Z. Adsorption of gases from SF_6 decomposition on aluminum-doped SWCNTs: A density functional theory study. The European Physical Journal D. 2015;**69:**1-8

[33] Azizi K, Karimpanah M. Computational study of Al- or P-doped single-walled carbon nanotubes as NH_3 and NO_2 sensors. Applied Surface Science. 2013;**285:**102-109

[34] Zhang X, Chen Q, Tang J, et al. Adsorption of SF_6 decomposed gas on anatase (101) and (001) surfaces with oxygen defect: a density functional theory study [J]. Scientific Reports, 2014, **4**(4):4762.

[35] Zhang X, Chen Q, Hu W. Zhang J. A DFT study of SF_6 decomposed gas adsorption on an anatase (101) surface. Applied Surface Science. 2013;**286:**47-53

[36] Sammells AF, Schwartz M, Mackay RA, Barton TF, Peterson DR. Catalytic membrane reactors for spontaneous synthesis gas production. Catalysis Today. 2000;**56:**325-328

[37] Zhang X, Gui Y, Dai Z. A simulation of Pd-doped SWCNTs used to detect SF_6 decomposition components under partial discharge. Applied Surface Science. 2014;**315:**196-202

[38] Pan X, Cai Q-x, Chen W-l, Zhuang G-l, Li X-n, Wang J-g. A DFT study of gas molecules adsorption on the anatase (001) nanotube arrays. Computational Materials Science. 2013;**67:**174-181

[39] Reddy EL, Biju VM, Subrahmanyam C. Production of hydrogen from hydrogen sulfide assisted by dielectric barrier discharge. International Journal of Hydrogen Energy. 2012;**37:**2204-2209

[40] Mubeen S, Zhang T, Chartuprayoon N, et al. Sensitive Detection of H2S Using Gold Nanoparticle Decorated Single-Walled Carbon Nanotubes[J]. Analytical Chemistry, 2010, **82**(1):250-7.

[41] Sanderson RT. Electronegativity and bond energy. Journal of the American Chemical Society. 1983;**105:**2259-2261

[42] Casanovas AM, Casanovas J, Dubroca V, Lagarde F, Belarbi A. Optical detection of corona discharges in SF_6, CF_4, and SO_2 under dc and 50-Hz ac voltages. Journal of Applied Physics. 1991;**70:**1220-1226

[43] Kohn W, Becke AD, Parr RG. Density functional theory of electronic structure. The Journal of Physical Chemistry. 1996;**100:**12974-12980

[44] McNicholas TP, Zhao K, Yang C, Hernandez SC, Mulchandani A, Myung NV, Deshusses MA. Sensitive detection of elemental mercury vapor by gold-nanoparticle-decorated carbon nanotube sensors. The Journal of Physical Chemistry C. 2011;**115:**13927-13931

[45] Xiaoxing Z, Fansheng M, Zhen W, Jian L. Gas-sensing simulation of single-walled carbon nanotubes applied to detect gas decomposition products of SF_6 in PD. In: Electrical Insulation Conference (EIC), 2011, Vol. 2011, pp. 132-135

[46] Park Y, Lahaye RJWE, Lee YH. Adsorption of Pt on defective carbon nanotube walls: A DFT approach. Computer Physics Communications. 2007;**177**:46

[47] Pannopard P, Khongpracha P, Probst M, Limtrakul J. Gas sensing properties of platinum derivatives of single-walled carbon nanotubes: A DFT analysis. Journal of Molecular Graphics & Modelling. 2009;**28:**62-69

[48] Zhang X, Dai Z, Chen Q, Tang J. A DFT study of SO_2 and H_2S gas adsorption on Au-doped single-walled carbon nanotubes. Physica Scripta. 2014;**89:**065803